Simulation studies of $R_2(\Delta\eta, \Delta\varphi)$ and $P_2(\Delta\eta, \Delta\varphi)$ correlation functions in pp collisions with the PYTHIA and HERWIG models

Baidyanath Sahoo,[1,*] Basanta Kumar Nandi,[1] Prabhat Pujahari,[2] Sumit Basu,[3,†] and Claude Pruneau[3,‡]

[1]*Department of Physics, Indian Institute of Technology Bombay, Mumbai-400076, India*

[2]*Department of Physics, Indian Institute of Technology Madras, Chennai-600025, India*

[3]*Department of Physics and Astronomy, Wayne State University, Detroit, Michigan 48201, USA*

(Received 24 October 2018; revised manuscript received 11 June 2019; published 21 August 2019)

We report studies of charge-independent (CI) and charge-dependent (CD) two-particle differential-number correlation functions, $R_2(\Delta\eta, \Delta\varphi)$, and transverse momentum (p_T) correlation functions, $P_2(\Delta\eta, \Delta\varphi)$, of charged particles in $\sqrt{s} = 2.76$ TeV pp collisions with the PYTHIA and HERWIG models. Model predictions are presented for inclusive charged hadrons ($h^{\pm}$), as well as pions ($\pi^{\pm}$), kaons ($K^{\pm}$), and (anti-)protons ($\bar{p}/p$) in the ranges $0.2 < p_T \leqslant 2.0\,\mathrm{GeV}/c$, $2.0 < p_T \leqslant 5.0\,\mathrm{GeV}/c$, and $5.0 < p_T \leqslant 30.0\,\mathrm{GeV}/c$, with full azimuthal coverage in the range $|\eta| < 1.0$. We compare the model predictions for the strength and shape of the R_2 and P_2 correlators as these pertain to recent measurements by the ALICE collaboration. The R_2 and P_2 correlation functions estimated with PYTHIA and HERWIG exhibit qualitatively similar near-side and away-side correlation structures but feature important differences. Our analysis indicates that comparative studies of R_2 and P_2 correlation functions would provide valuable insight towards the understanding of particle production in pp collisions, and by extension, should also be useful in studies of heavy-ion collisions. Comparison of the $\Delta\eta$ dependence of R_2 and P_2 could contribute, in particular, to a better understanding and modeling of the angular ordering of particles produced by hadronization in jets, as well as a better description of jet fragmentation functions of identified species at low momentum fraction (z).

DOI: 10.1103/PhysRevC.100.024909

I. INTRODUCTION

Measurements of integral and differential correlation functions constitute essential tools for the study of proton-proton (pp) and heavy-ion (A–A) collisions at relativistic energies. Two- and multiparticle azimuthal correlations functions have provided evidence for the existence of anisotropic flow in A–A collisions [1–7], quark scaling (approximate) of flow coefficients in A–A collisions at RHIC and LHC [8–11]. They were also used to investigate the presence of flow in smaller systems (e.g., p–A and high multiplicity pp collisions) [12–17]. Differential two-particle (number) correlation functions additionally enabled the discovery of jet quenching at RHIC [18,19] and its detailed characterization in A–A collisions at both RHIC and LHC [20]. Several other correlation functions, including number and transverse momentum correlation functions [21,22] have been measured and investigated both at RHIC and LHC to better understand the particle production dynamics and study the properties of the matter produced in pp and A–A collisions [23–28]. Among these, the recent measurements of number correlation, R_2, and differential transverse momentum correlation, P_2, defined in Sec. II, have enabled independent confirmation of the collective nature of the azimuthal correlations observed in Pb–Pb collisions [29], as well as the identification of noticeable differences in the $\Delta\eta$ and $\Delta\varphi$ dependence of these correlation functions [28]. These measurements show that the near-side peak of both CI and CD correlations is significantly narrower, at any given A–A collision centrality in P_2 than in R_2 correlation functions. This confirms [30] that comparative measurements of P_2 and R_2 correlation functions may provide additional sensitivity to the underlying particle production mechanisms in heavy-ion collisions. In this work, we seek to establish whether the difference observed in Ref. [28] can be readily explained by jet contributions. To this end, we examine predictions of the R_2 and P_2 correlation functions by the PYTHIA [31] and HERWIG [32] models that are known to quantitatively reproduce many jet related observables reported and compiled by RHIC and LHC experiments [33–35]. We examine the differential correlation functions R_2 and P_2 in pp collisions with a particular focus on particles produced in the range $0.2 < p_T \leqslant 2.0$ GeV/c reported by ALICE [28,29] but also extend our study to include higher momentum ranges to further examine how the two observables behave for higher particle momenta expected to be dominated by jet production.

Particle production in high-energy nucleus-nucleus collisions is governed by several conservation laws including (electric) charge conservation, baryon number conservation, strangeness conservation, as well as energy-momentum conservation. At very large collision energy, the yield of anti-particles and particles are nearly equal. Limited information

*baidya@iitb.ac.in

†sumit.basu@cern.ch

‡claude.pruneau@wayne.edu

is thus gained by studying the yields, e.g., π^+ and π^- individually. Additional insight may be provided, however, by comparative studies of like-sign (LS) and unlike-sign (US) particle pairs, e.g., π^+, π^+ and π^+, π^-, or baryon-baryon and baryon-anti-baryon particle pairs. We thus study predictions of the models for both charge-independent (CI) and charge-dependent (CD) pair combinations.

This paper is organized as follows. Section II presents definitions of the R_2 and P_2 correlation functions studied in this work and describes how they are computed. The PYTHIA and HERWIG models, and the conditions under which they were used to generate pp events, are briefly described in Sec. III. Predictions by the models for R_2 and P_2 correlation functions are presented in Sec. IV, and conclusions are summarized in Sec. V.

II. CORRELATION FUNCTIONS DEFINITION

The R_2 and P_2 correlation functions are defined in terms of single- and two-particle densities expressed as functions of the particle pseudorapidity η and azimuthal angle φ,

$$\rho_1(\eta, \varphi) = \frac{1}{\sigma_1}\frac{d^2\sigma_1}{d\eta d\varphi}, \tag{1}$$

$$\rho_2(\eta_1, \varphi_1, \eta_2, \varphi_2) = \frac{1}{\sigma_2}\frac{d^4\sigma_2}{d\eta_1 d\varphi_1 d\eta_2 d\varphi_2}, \tag{2}$$

where σ_1 and σ_2 are single and two-particle cross-sections, respectively. The correlator R_2 is defined as a two-particle cumulant normalized by the product of single-particle densities (hereafter called normalized two-particle cumulant) according to

$$R_2(\eta_1, \varphi_1, \eta_2, \varphi_2) = \frac{\rho_2(\eta_1, \varphi_1, \eta_2, \varphi_2)}{\rho_1(\eta_1, \varphi_1)\rho_1(\eta_2, \varphi_2)} - 1, \tag{3}$$

while the P_2 correlation function is defined in terms of the differential correlator $\langle \Delta p_T \Delta p_T \rangle$ normalized by the square of the average transverse momentum, p_T, to make it dimensionless, as follows:

$$P_2(\eta_1, \varphi_1, \eta_2, \varphi_2) = \frac{\langle \Delta p_T \Delta p_T \rangle(\eta_1, \varphi_1, \eta_2, \varphi_2)}{\langle p_T \rangle^2}. \tag{4}$$

The $\langle \Delta p_T \Delta p_T \rangle$ differential correlator [30] is defined according to

$$\langle \Delta p_T \Delta p_T \rangle(\eta_1, \varphi_1, \eta_2, \varphi_2) = \frac{\int_{p_{T,\min}}^{p_{T,\max}} \Delta p_{T,1} \Delta p_{T,2}\, \rho_2(\vec{p}_1, \vec{p}_2)\, dp_{T,1} dp_{T,2}}{\int_{p_{T,\min}}^{p_{T,\max}} \rho_2(\vec{p}_1, \vec{p}_2)\, dp_{T,1} dp_{T,2}}, \tag{5}$$

where $\Delta p_{T,i} = p_{T,i} - \langle p_T \rangle$ and $\langle p_T \rangle$ is the inclusive mean transverse momentum

$$\langle p_T \rangle = \frac{\int_{p_{T,\min}}^{p_{T,\max}} \rho_1 p_T dp_T}{\int_{p_{T,\min}}^{p_{T,\max}} \rho_1 dp_T}. \tag{6}$$

In addition to its sensitivity to the presence of particle correlations, P_2 is also determined by the momentum of the correlated particles [29]. It is positive whenever particle pairs emitted at specific azimuthal angle and pseudo-rapidity differences are more likely to both have transverse momenta higher (or lower) than the $\langle p_T \rangle$ and negative when a high-p_T particle ($p_T > \langle p_T \rangle$) is more likely to be accompanied by a low-p_T particle ($p_T < \langle p_T \rangle$). For instance, particles emitted within a jet typically have higher p_T than the inclusive average. Jets, therefore, contribute a large positive value to P_2. Hanbury-Brown and Twiss (HBT) correlations, determined by pairs of identical particles with $p_{T,1} \approx p_{T,2}$ should likewise contribute positively to this correlator. However, particle production involving a mix of low- and high-momenta correlated particles can contribute both positively and negatively. Based on this simple observation, one expects the internal structure of jets to influence the $\Delta\eta$, $\Delta\varphi$ dependence of the near-side peak of P_2 correlation functions. Within jets, as schematically illustrated in Fig. 1, high-p_T particles are predominantly emitted at small polar angles relative to the jet axis, while lower p_T particles span a larger angular range. This leads to an effective ordering of the particles (typical) p_T relative to the polar angle θ. In turn, this also leads to an effective p_T ordering in the $\Delta\eta$ versus $\Delta\varphi$ plane. For instance, one expects that for small $\Delta\eta$, $\Delta\varphi$ separations, high-p_T particles (i.e., $p_{T,i} \gg \langle p_T \rangle$) should dominate the P_2 correlation and contribute positive $\Delta p_T \Delta p_T$ values. Likewise, at very large $\Delta\eta$, $\Delta\varphi$ separation, the correlation strength should be determined by particle pairs with $p_{T,i} < \langle p_T \rangle$ thereby also yielding positive $\Delta p_T \Delta p_T$ values. However, there shall also be an intermediate $\Delta\eta$, $\Delta\varphi$ range such that pairs consist of one high-p_T particle and one low-p_T particle yielding negative $\Delta p_T \Delta p_T$

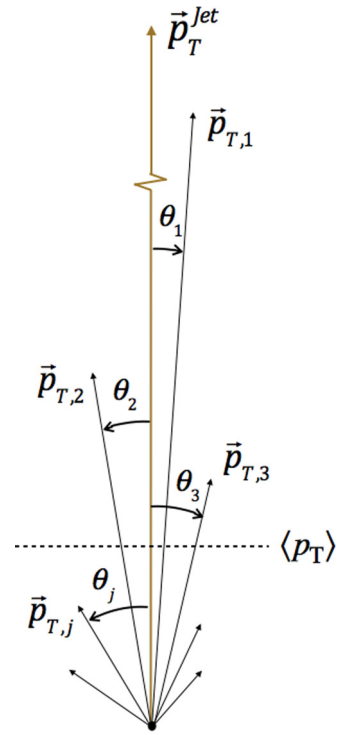

FIG. 1. Schematic representation of the transverse momentum and angular ordering of jet constituents relative to the jet axis, $\vec{p}_T^{\,Jet}$.

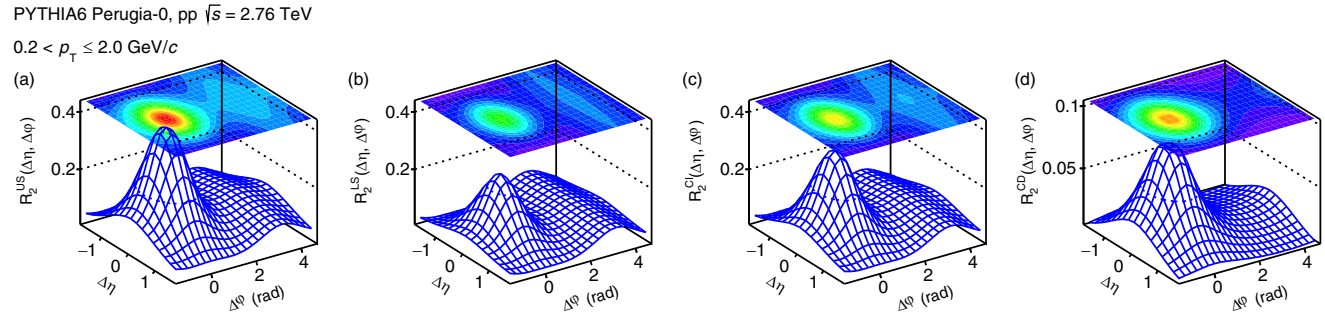

FIG. 2. Normalized two-particle cumulants (a) R_2^{US}, (b) R_2^{LS}, (c) R_2^{CI}, (d) R_2^{CD} obtained from PYTHIA simulations of pp collisions at $\sqrt{s} = 2.76$ TeV for charged hadrons in the pseudorapidity range $|\eta| < 1.0$ and the transverse momentum range $0.2 < p_T \leqslant 2.0$ GeV/c.

values on average. This should thus produce a narrowing and possibly a non-monotonic $\Delta\eta$, $\Delta\varphi$ dependence of the correlation strength. We shall demonstrate, in the following, that both PYTHIA and HERWIG do, in fact, exhibit such behavior.

In this work, the correlators R_2 and P_2 are reported as function of the differences $\Delta\eta = \eta_1 - \eta_2$ and $\Delta\varphi = \varphi_1 - \varphi_2$ by averaging across the mean pseudorapidity $\bar{\eta} = \frac{1}{2}(\eta_1 + \eta_2)$ and the mean azimuthal angle $\bar{\varphi} = \frac{1}{2}(\varphi_1 + \varphi_2)$ acceptance according to

$$\mathrm{O}(\Delta\eta, \Delta\varphi) = \frac{1}{\Omega(\Delta\eta)} \int \mathrm{O}(\eta_1, \varphi_1, \eta_2, \varphi_2)\delta(\Delta\varphi - \varphi_1 + \varphi_2)d\varphi_1 d\varphi_2 \times \delta(\Delta\eta - \eta_1 + \eta_2)d\eta_1 d\eta_2, \quad (7)$$

where $\Omega(\Delta\eta)$ represents the width of the acceptance in $\bar{\eta}$ at a given value of $\Delta\eta$ and angle differences $\Delta\varphi$ are

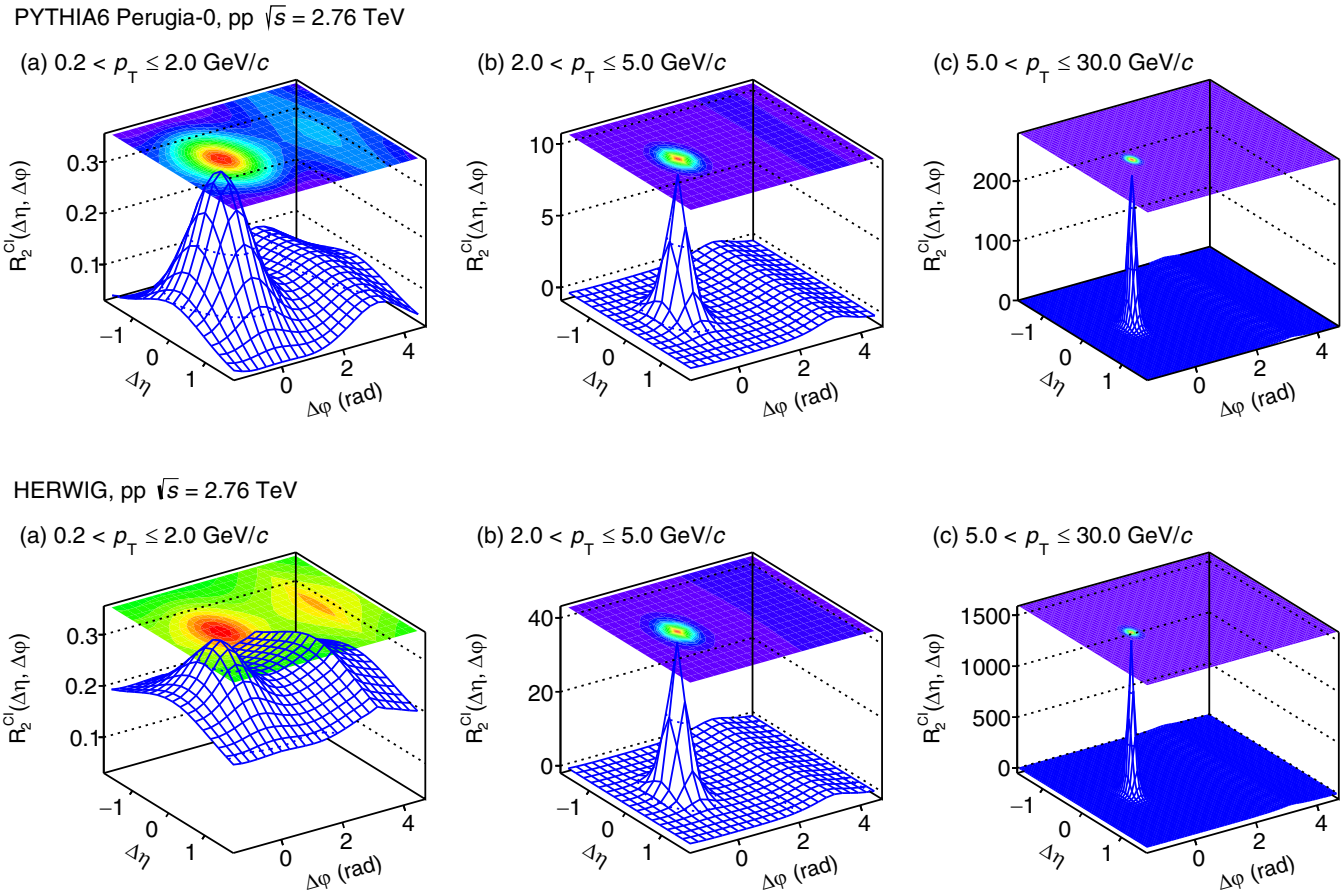

FIG. 3. Correlation functions R_2^{CI} of charged hadrons, in selected p_T ranges, obtained with PYTHIA (top panel) and HERWIG (bottom panel) in pp collisions at $\sqrt{s} = 2.76$ TeV.

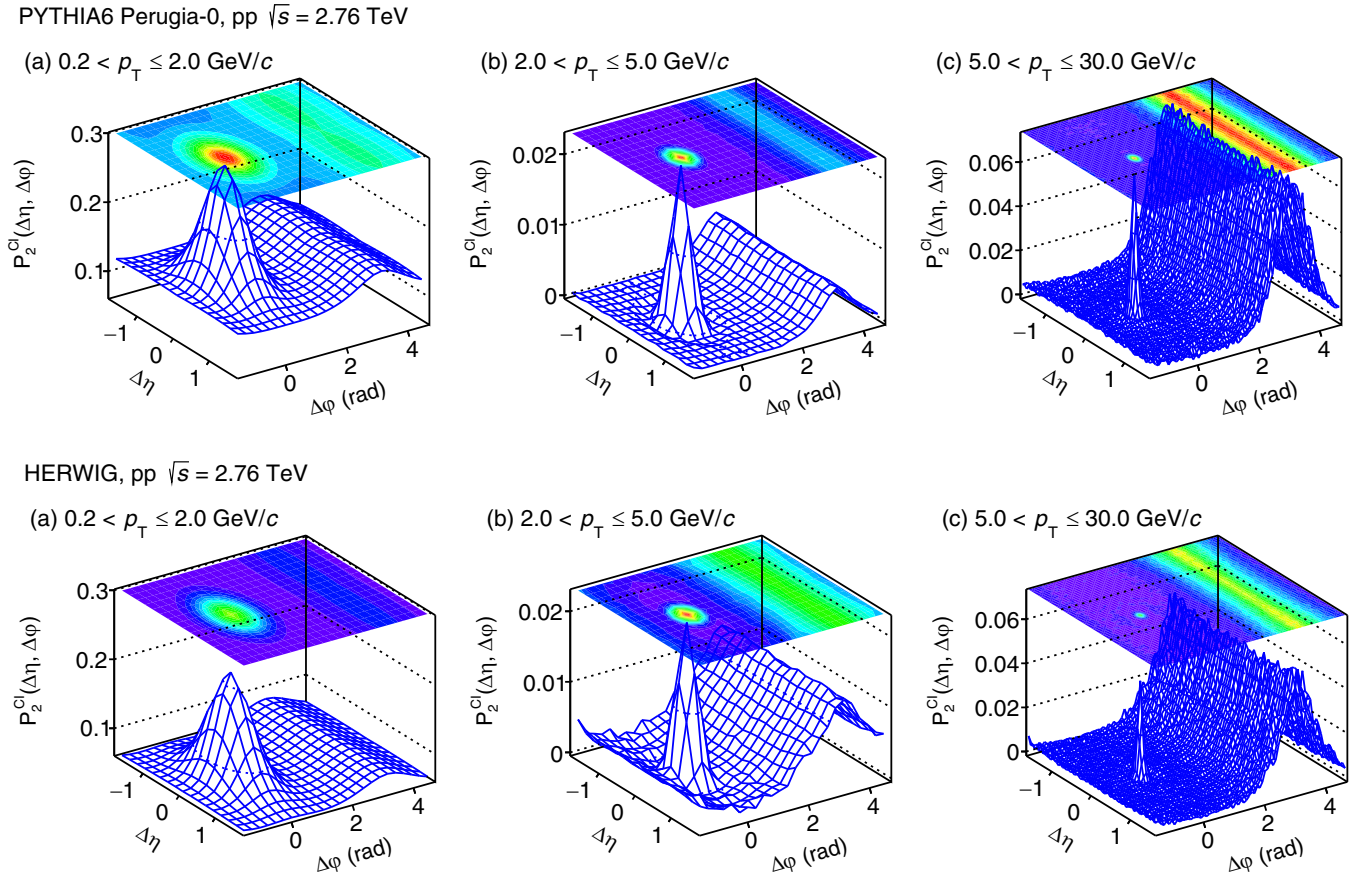

FIG. 4. Correlation functions P_2^{CI} of charged hadrons, in selected p_T ranges, obtained with PYTHIA (top panel) and HERWIG (bottom panel) in pp collisions at $\sqrt{s} = 2.76$ TeV.

calculated modulo 2π and shifted by $-\pi/2$ for convenience of representation in the figures. The analysis of the R_2 and P_2 correlation functions are carried out for charge combination pairs $(+-)$, $(-+)$, $(++)$, and $(--)$ separately. Like-sign pairs correlations are averaged to yield LS correlations, $O^{LS} = \frac{1}{2}[O^{++} + O^{--}]$, and US correlators are obtained by averaging $(+-)$ and $(-+)$ correlations, $O^{US} = \frac{1}{2}[O^{+-} + O^{-+}]$. The LS and US correlations are then combined to yield charge-independent and charge-dependent correlation functions according to

$$O^{CI} = \tfrac{1}{2}[O^{US} + O^{LS}], \tag{8}$$

$$O^{CD} = \tfrac{1}{2}[O^{US} - O^{LS}]. \tag{9}$$

The CI correlation function measures the average of all correlations between charged particles while the CD correlation function is sensitive to the difference of US and LS pairs and is largely driven, as such, by charge conservation effects. The CD correlation function is proportional to the charge balance function [23] when the yields of positive and negative particles are equal [36].

We repeated the analysis and used the sub-sampling technique to obtain a more accurate estimation of statistical uncertainty. The Monte Carlo data sample was divided into 10 segments of equal size—e.g., equal number of events. Each subsample was analyzed independently. We then extracted the mean values and calculated the sample standard deviations (σ) according to

$$\sigma = \sqrt{\frac{\sum_i (O_i - \langle O \rangle)^2}{N-1}}, \tag{10}$$

where "N-1" used instead of "N" depending on Bessel's correction and, where i= 1,2,...10. The error on the mean is calculated bin-by-bin using the general formula $\sigma_{\text{error}} = \frac{\sigma}{\sqrt{N}}$.

III. MONTE CARLO MODELS

The impact of jet production on R_2 and P_2 correlation functions in pp is studied with Monte Carlo simulations carried out with the event generators PYTHIA 6.425, tune Perugia-0 [31,37–40], and HERWIG 6.5 [32]. PYTHIA and HERWIG are both based on QCD at Leading Order (LO) but use different parton production and hadronization schemes. PYTHIA uses the Lund string fragmentation model for high-p_T parton hadronization while the production of soft particles (i.e., the underlying event) is handled through fragmentation of mini-jets from initial and final state radiation, multiple parton interactions (MPI), and proton remnants [41]. The kPyJets process responsible for jet production uses the CTEQ6l [42] parametrization of the proton parton distribution function (PDF) tuned for LHC energies. HERWIG events were

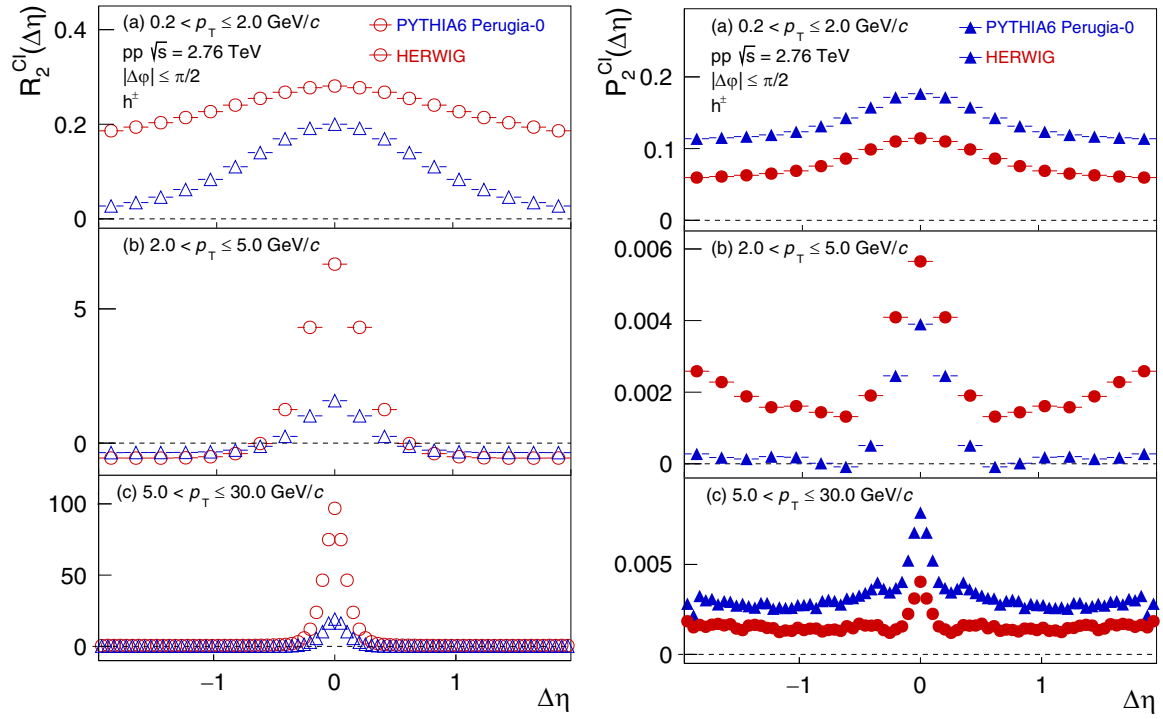

FIG. 5. Projections onto $\Delta\eta$ of the R_2^{CI} (left panel) and P_2^{CI} (right panel) correlation functions calculated with PYTHIA (blue) and HERWIG (red) for $h^{\pm}$ in pp collisions at $\sqrt{s} = 2.76$ TeV in selected p_T ranges. The $\Delta\eta$ projections are calculated as averages of the two-dimensional correlations in the ranges $|\Delta\varphi| \leqslant \pi/2$.

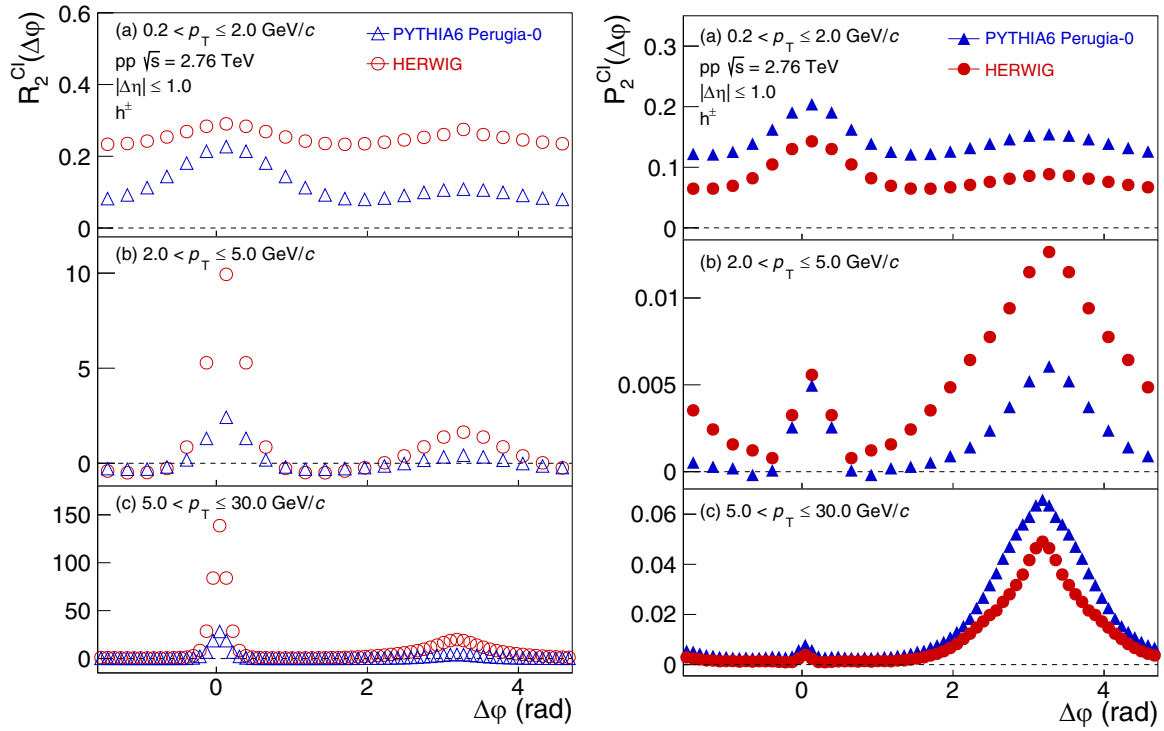

FIG. 6. Projections onto $\Delta\varphi$ of R_2^{CI} (left panel) and P_2^{CI} (right panel) correlation functions calculated with PYTHIA (blue) and HERWIG (red) for $h^{\pm}$ in pp collisions at $\sqrt{s} = 2.76$ TeV in selected p_T ranges. The $\Delta\varphi$ projections are calculated as averages of the two-dimensional correlations in the ranges $|\Delta\eta| \leqslant 1.0$.

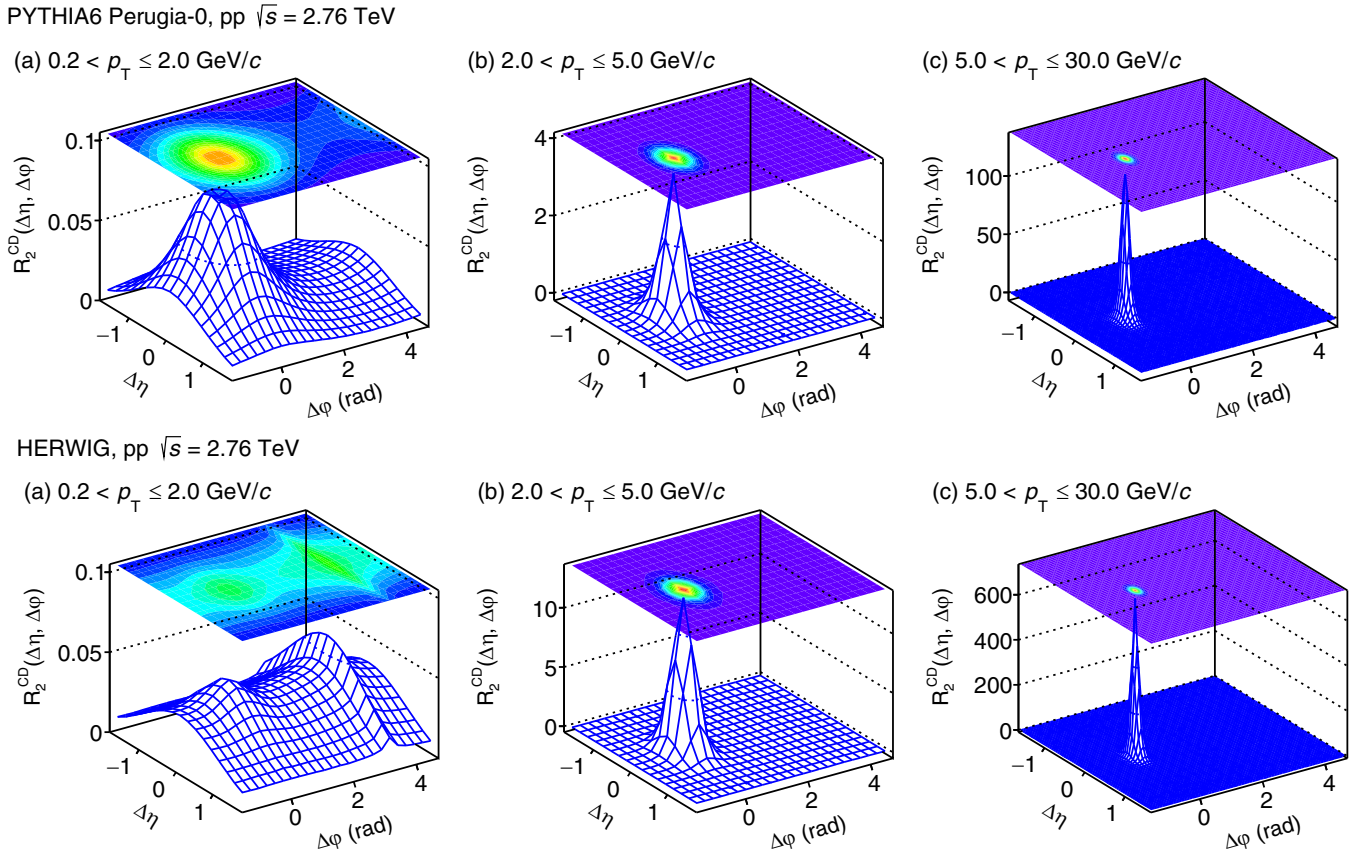

FIG. 7. Correlation functions R_2^{CD} of charged hadrons, in selected p_T ranges, obtained with PYTHIA (top panel) and HERWIG (bottom panel) in pp collisions at $\sqrt{s} = 2.76$ TeV.

generated based on the jet generation process 1500 [32] and the CTEQ5L [43] parametrization of the proton PDFs with hard color-singlet exchange between two partons [44] using leading-logarithmic (LL) BFKL [45] calculations in ALICE environment. In HERWIG, the perturbative parton evolution ends with the production of clusters subsequently decayed into final-state hadrons.

To study the correlation functions with reliable statistical accuracy, and given the jet production cross-section falls steeply with increasing transverse momentum, we generated equal number of PYTHIA and HERWIG events in three hard QCD ($2 \rightarrow 2$ processes) $\hat{p}_T$ bins: 5.0–10.0 GeV/c, 10.0–20.0 GeV/c, and 20.0–30.0 GeV/c [46]. A total of 2×10^8 events were generated with PYTHIA and 2×10^8 HERWIG events were produced in each $\hat{p}_T$ bins. Single- and two-particle densities were calculated independently in each $\hat{p}_T$ bin and averaged with weights corresponding to their respective fractional cross-sections.

Charge, baryon number, or strangeness balance function [23] are of interest to study the role of conservation laws and the dynamics of particle transport in elementary and heavy-ion collisions. However, charge balance functions should be proportional and thus equivalent to the correlator R_2^{CD} provided the measured multiplicities of positively and negatively charged particles are equal. We verified the applicability of the equivalence by comparing the differential cross-sections of positively and negatively charged hadrons, $h^{\pm}$, and found that the ratio of cross-sections is of order unity in the p_T range of interest of this study. It is then legitimate to use the

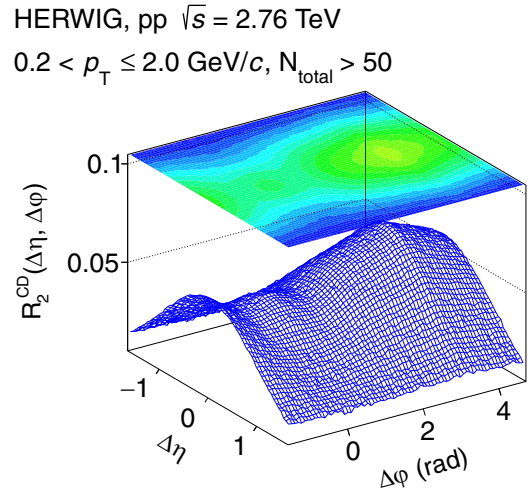

FIG. 8. Correlation function R_2^{CD} obtained with HERWIG for charged hadrons in pp collisions at $\sqrt{s} = 2.76$ TeV with a minimum multiplicity cut, $N_{total} > 50$.

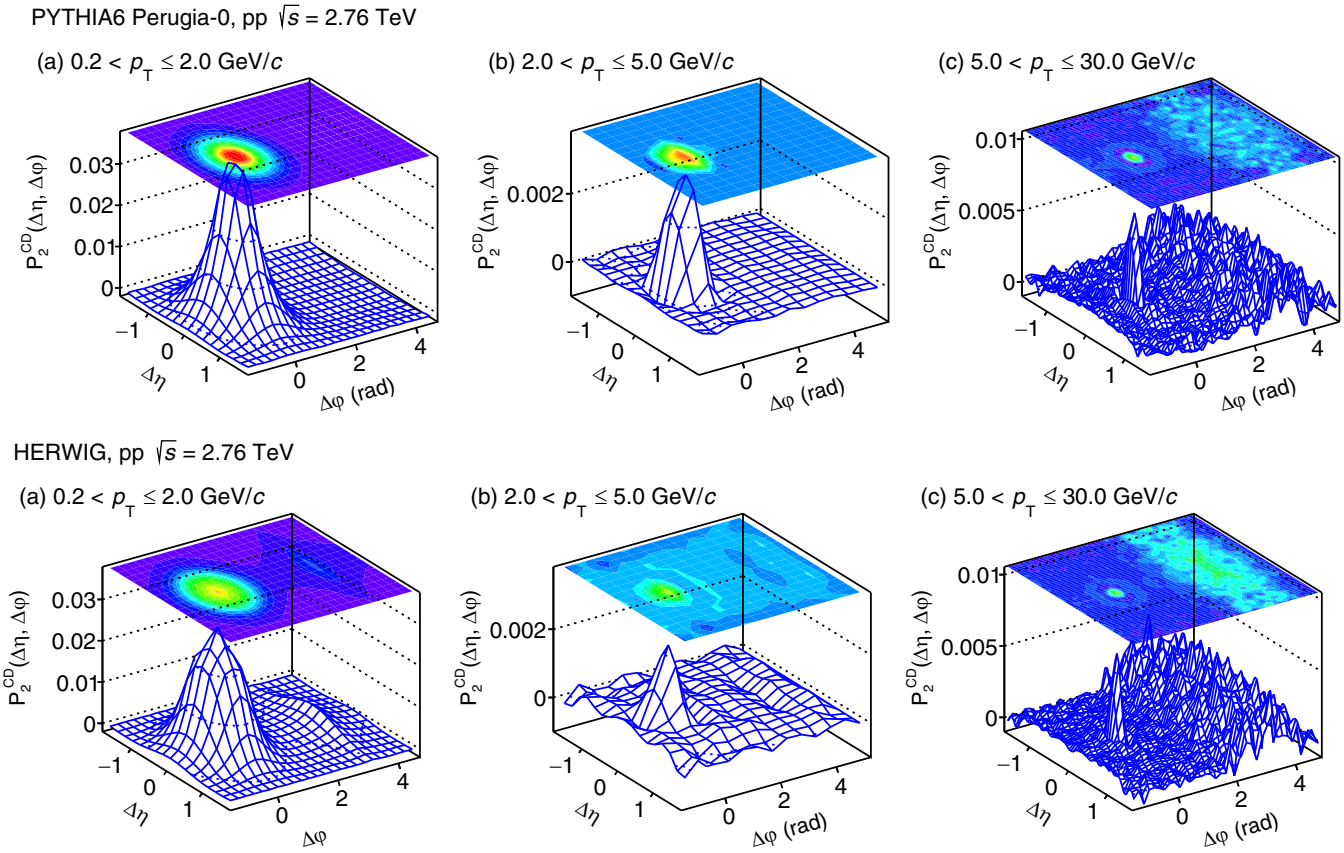

FIG. 9. Correlation functions P_2^{CD} of charged hadrons, in selected p_T ranges, obtained with PYTHIA (top panel) and HERWIG (bottom panel) in pp collisions at $\sqrt{s} = 2.76$ TeV.

R_2^{CD} correlation function as a proxy for the balance function: balance functions are thus not explicitly reported in this study.

IV. MODEL PREDICTIONS

We begin with a discussion of unidentified charged hadron correlation functions in Sec. IV A. Correlation functions for identified particles, e.g., pions, kaons, and protons, are presented in Sec. IV C.

A. Inclusive charged hadron correlations

We focus our discussion on CI and CD correlation functions. Associated balance functions, B, can be obtained by multiplying R_2^{CD} correlation functions with integrals of the hadron cross-sections. Figure 2 illustrates the calculation of CI and CD correlation functions based on the correlators R_2^{US} and R_2^{LS}. Figures 2(a) and 2(b) present examples of these correlation functions calculated with PYTHIA for particles in the transverse momentum range $0.2 < p_T \leqslant 2.0$ GeV/c and pseudorapidity range $|\eta| < 1.0$. The US and LS correlation functions are combined according to Eqs. (8) and (9) to obtain CI and CD correlation functions shown in Figs. 2(c) and 2(d) of the same figure.

The US and LS correlation functions both feature a prominent near-side peak centered at $(\Delta\eta, \Delta\varphi) = (0, 0)$. One notes, however, that the peak observed in US correlation functions is taller than that observed in LS correlation functions. This leads to a modest and narrow near-side peak in the CD correlation function shown in Fig. 2(d). The amplitude and shape of this peak are determined by the (charge) pair production and hadronization processes. We show in this article that PYTHIA and HERWIG make quantitatively different predictions of these features. Measurements of R_2^{CD} correlation functions shall thus provide a valuable basis to test the underlying mechanisms used in these models for $q\bar{q}$ pair creation and hadronization of partons into hadrons, $q(\bar{q}) \to h^{\pm}$.

1. Charge independent correlations

We first compare the R_2 and P_2 correlation functions for CI charge combinations obtained in simulations of pp collisions with the PYTHIA and HERWIG generators. Figures 3 and 4 present the R_2^{CI} and P_2^{CI} correlation functions, respectively.

Correlation functions are presented for unidentified charged hadrons calculated in momentum ranges: (i) $0.2 < p_T \leqslant 2.0$ GeV/c, (ii) $2.0 < p_T \leqslant 5.0$ GeV/c, and (iii) $5.0 < p_T \leqslant 30.0$ GeV/c. In these and the following figures, the $\langle p_T \rangle$ values used for the calculation of $\Delta p_T \Delta p_T$ are the p_T averages of particles produced in each of these three ranges, respectively. The first momentum range samples the underlying event in pp collisions and is relevant for comparisons with bulk particle production in A–A collisions. The second range corresponds to the coalescence range [47,48], while

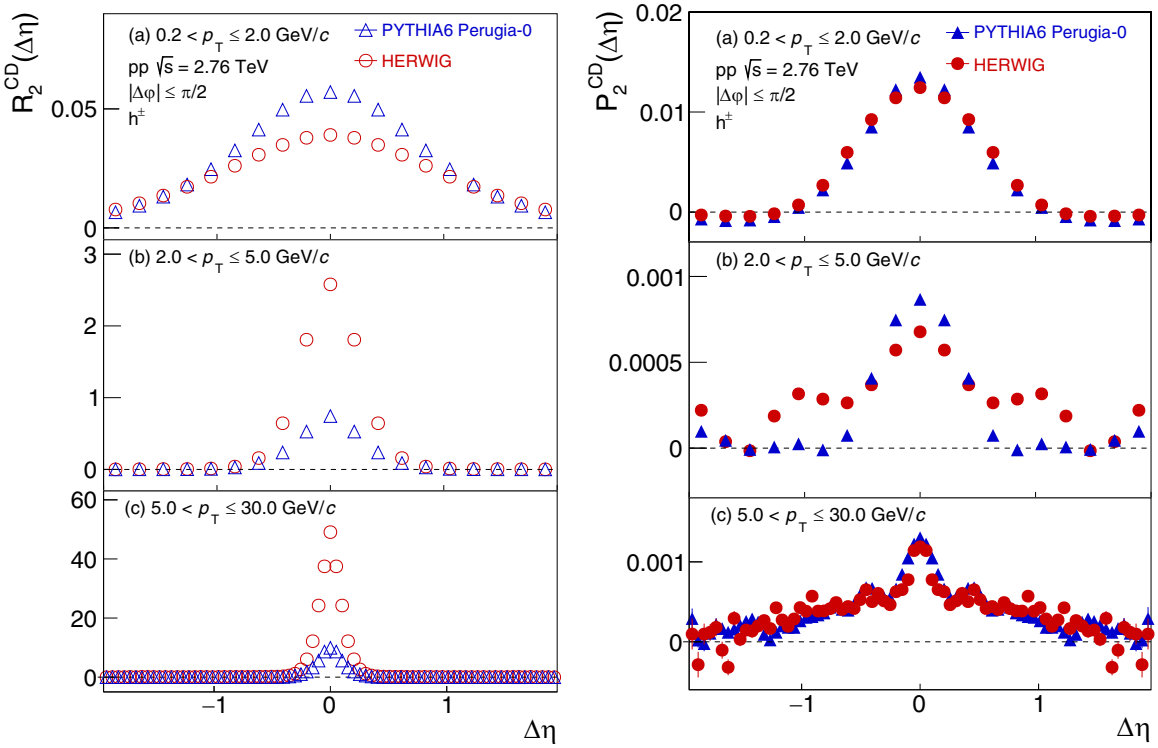

FIG. 10. Projections onto $\Delta\eta$ of R_2^{CD} (left column) and P_2^{CD} (right column) correlation functions of charged hadrons calculated in selected p_T ranges with PYTHIA (blue) and HERWIG (red) in pp collisions at $\sqrt{s} = 2.76$ TeV. The projections are calculated as averages of the two-dimensional correlations in the range $|\Delta\varphi| \leqslant \pi/2$.

the third range shifts the focus on particles produced by jet fragmentation. We find calculations of the R_2 and P_2 correlation functions in these three ranges yield qualitatively similar results. However, they also exhibit interesting quantitative differences which we discuss in details, in the following, based on projections onto the $\Delta\eta$ and $\Delta\varphi$ axes. The R_2^{CI} and P_2^{CI} correlation functions feature a prominent near-side peak centered at $(\Delta\eta, \Delta\varphi) = (0, 0)$ as well as an away-side structure, centered at $\Delta\varphi = \pi$, and extending across the range $|\Delta\eta| \leqslant 1.6$ (truncated in the figure to avoid the fluctuations at larger $\Delta\eta$). Such near-side and away-side features have been observed in triggered and non-triggered correlation function measured in a variety of collision systems and beam energies [14,19,28,29,49–51]. In this work, we study the predictions of the PYTHIA and HERWIG models relative to their dependence on the particle momenta, the particle species, and we focus, in particular, on the differences between R_2 and P_2 correlation functions.

In Figs. 3 and 4, one observes the longitudinal and azimuthal widths of the near-side peak of the R_2^{CI} and P_2^{CI} correlation functions predicted by the two models decrease monotonically with the p_T range of the particles. Additionally, the near-side peak of P_2^{CI} correlations are systematically narrower than those observed in the R_2^{CI} correlation functions, as reported by the ALICE collaboration [28,29]. These differences are studied quantitatively based on the projections of the correlation functions onto the $\Delta\eta$ and $\Delta\varphi$ axes presented in Figs. 5 and 6.

Projections of the R_2^{CI} and P_2^{CI} correlation functions onto the $\Delta\eta$ axis calculated with the PYTHIA and HERWIG models are presented in the left and right panels of Fig. 5, respectively, for the three p_T ranges already considered. One observes that the models make quantitatively different predictions for both correlation functions in all three p_T ranges. Indeed, both models yield peaks centered at $(\Delta\eta, \Delta\varphi) = (0, 0)$ but the shape and strength of these peaks differ markedly across models. The strengths and widths of the peaks also evolve differently with p_T. One notes, additionally, that the calculations for P_2^{CI} exhibit quite noticeable differences with R_2^{CI}: they feature narrower peaks and different ordering in the strengths predicted by the models. The RMS widths of these projections are plotted in Fig. 12 and discussed in more details in sec. IV B. It is clear at the outset, however, that measurements of both R_2^{CI} and P_2^{CI} in pp collisions with different p_T ranges should in principle provide significant constraints on the models and their underlying particle production mechanisms.

Caution in the interpretation of the widths of the near-side peak of the P_2^{CI} correlation functions is needed, however, because of the complicated dependence of the correlation strength on the distance to the centroid of the peak. One observes, in particular, that the correlation strength of P_2^{CI} exhibits an undershoot, in both $\Delta\eta$ and $\Delta\varphi$ projections, in the p_T range 2.0–5.0 GeV/c, and a longer range oscillatory behavior in projections of P_2^{CI} along $\Delta\eta$ in the p_T range 5.0–30.0 GeV/c, as expected from the angular ordering of

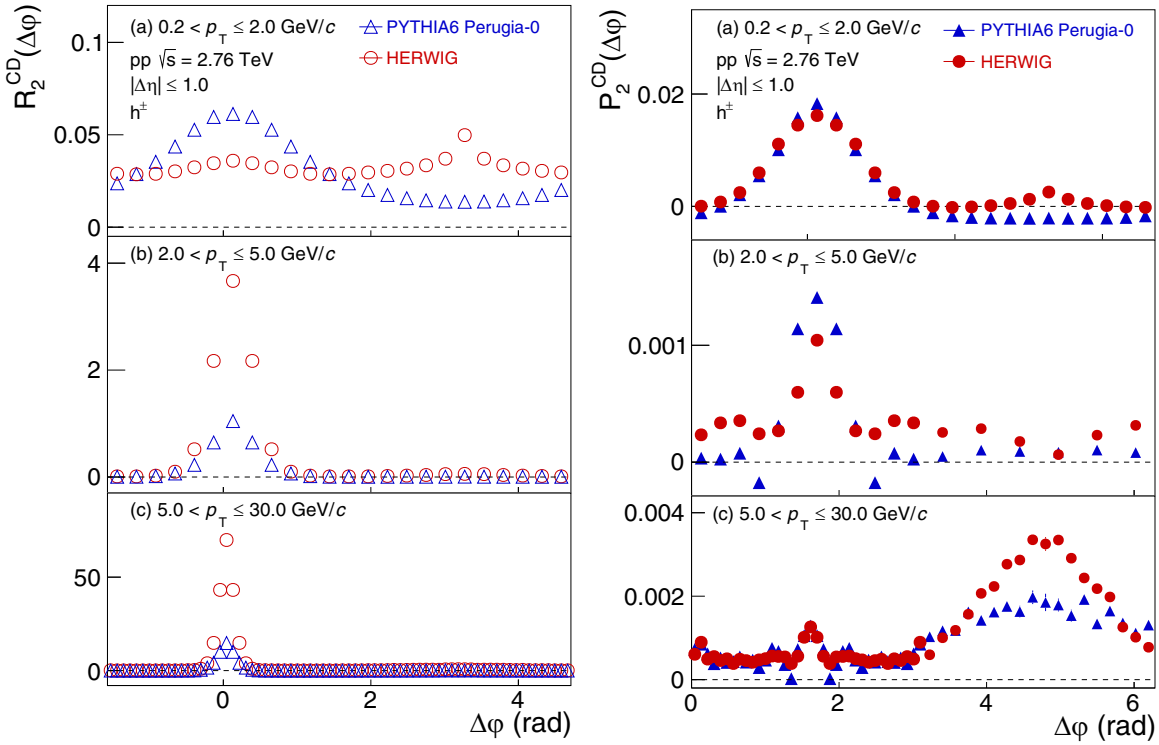

FIG. 11. Projections onto $\Delta\varphi$ of R_2^{CD} (left column) and P_2^{CD} (right column) correlation functions of charged hadrons calculated in selected p_T ranges with PYTHIA (blue) and HERWIG (red) in pp collisions at $\sqrt{s} = 2.76$ TeV. The $\Delta\varphi$ projections are calculated as averages of the two-dimensional correlations in the range $|\Delta\eta| \leqslant 1.0$.

particle p_T discussed in Sec. II. While difficult to resolve, a hint for the existence of such undershoot feature has already been reported in Ref. [28]. The presence of this undershoot stems from the explicit dependence of the correlator on the particles' transverse momentum deviation from the mean, i.e., $\Delta p_T \Delta p_T$. At short angular distance (both longitudinally and azimuthally), jet particles have momenta that tend to exceed the mean p_T and thus contribute positively, on average, to the correlator. The presence of the undershoot indicates that there is an angular range within which the product $\Delta p_T \Delta p_T$ is negative on average in PYTHIA events, but shifted in HERWIG events. The shift observed in HERWIG events likely results from larger event-by-event multiplicity fluctuations. At large angular separation, both particles tend to have p_T below the $\langle p_T \rangle$ and thus contribute positively to the P_2 correlator. The peak and oscillatory behavior are thus determined by the p_T and angular ordering of the jet constituents. Given PYTHIA and HERWIG produce particles using a different ordering, they are expected and indeed observed to yield different shapes for the P_2 correlation function. By contrast, the R_2 correlation function receives positive definite contributions from all particle pairs of a jet and is thus not sensitive to

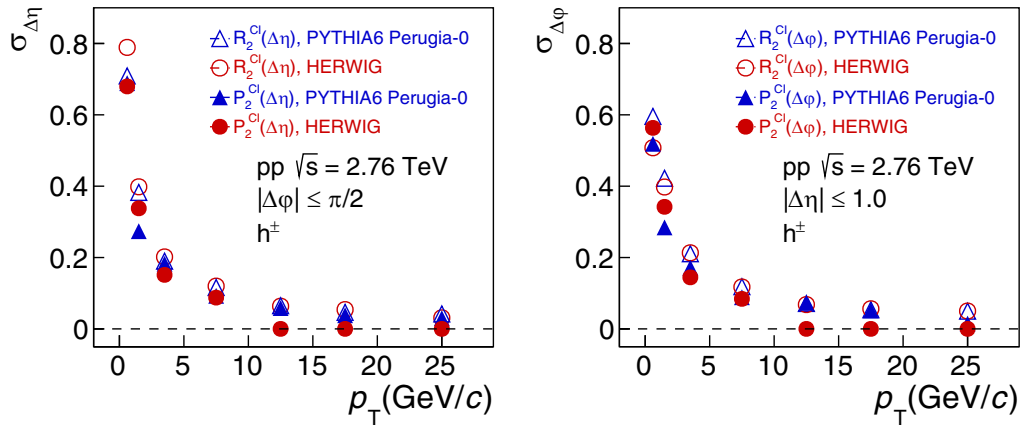

FIG. 12. Width of the near-side peak of CI correlation functions along $\Delta\eta$ (left panel), in the range $|\Delta\varphi| \leqslant \pi/2$, and along $\Delta\varphi$ (right panel), in the range $|\Delta\eta| \leqslant 1.0$, as function of the momentum of the particles.

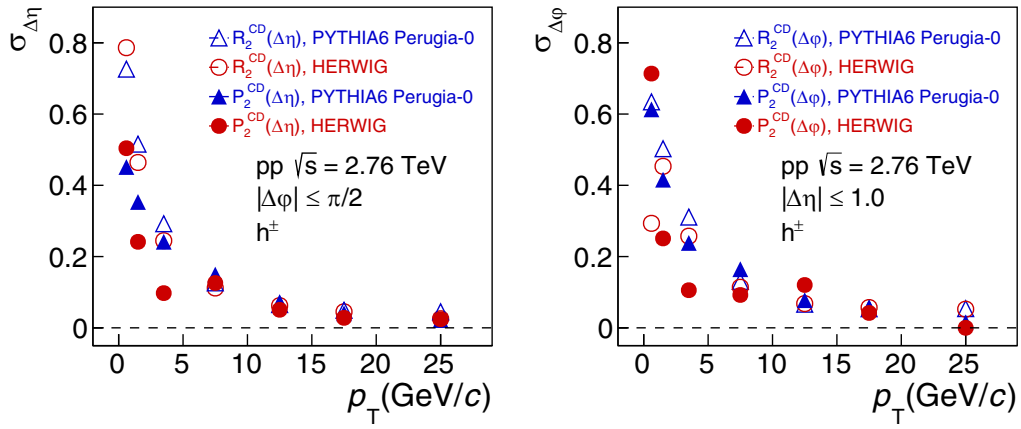

FIG. 13. Width of the near-side peak of CD correlation functions along $\Delta\eta$ (left panel), in the range $|\Delta\varphi| \leqslant \pi/2$, and along $\Delta\varphi$ (right panel), in the range $|\Delta\eta| \leqslant 1.0$, as function of the momentum of the particles.

the ordering of the particles of the pair but only the overall width of the jet. Measurements of R_2 and P_2 correlation functions in p–Pb and Pb–Pb collisions shall thus provide better discriminants of the parton splitting and hadronization mechanisms at play in jet fragmentation as well as in the generation of the underlying event.

The R_2^{CI} and P_2^{CI} correlations also exhibit stark differences on the away-side, i.e., at $\Delta\varphi \sim \pi$. Inspection of the away-side of the R_2 (Fig. 3) and P_2 correlation functions (Fig. 4), and their $\Delta\varphi$ projections (Fig. 6) reveal the two correlators yield a rather different response to the away-side jet. Indeed, the away-side jet yields a relatively modest ridge-like structure at

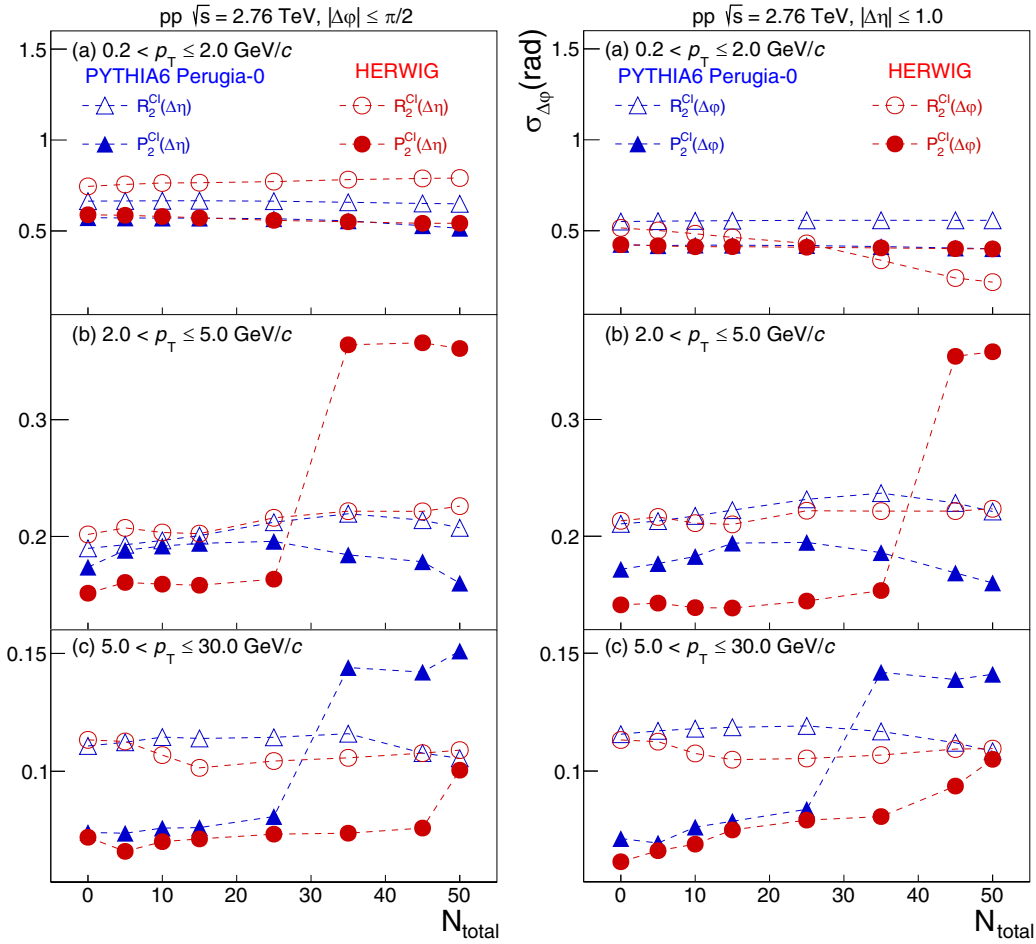

FIG. 14. Width of the near-side peak of CI correlation functions along $\Delta\eta$ (left panel), in the range $|\Delta\varphi| \leqslant \pi/2$, and along $\Delta\varphi$ (right panel), in the range $|\Delta\eta| \leqslant 1.0$. Dotted lines are drawn to guide the eye.

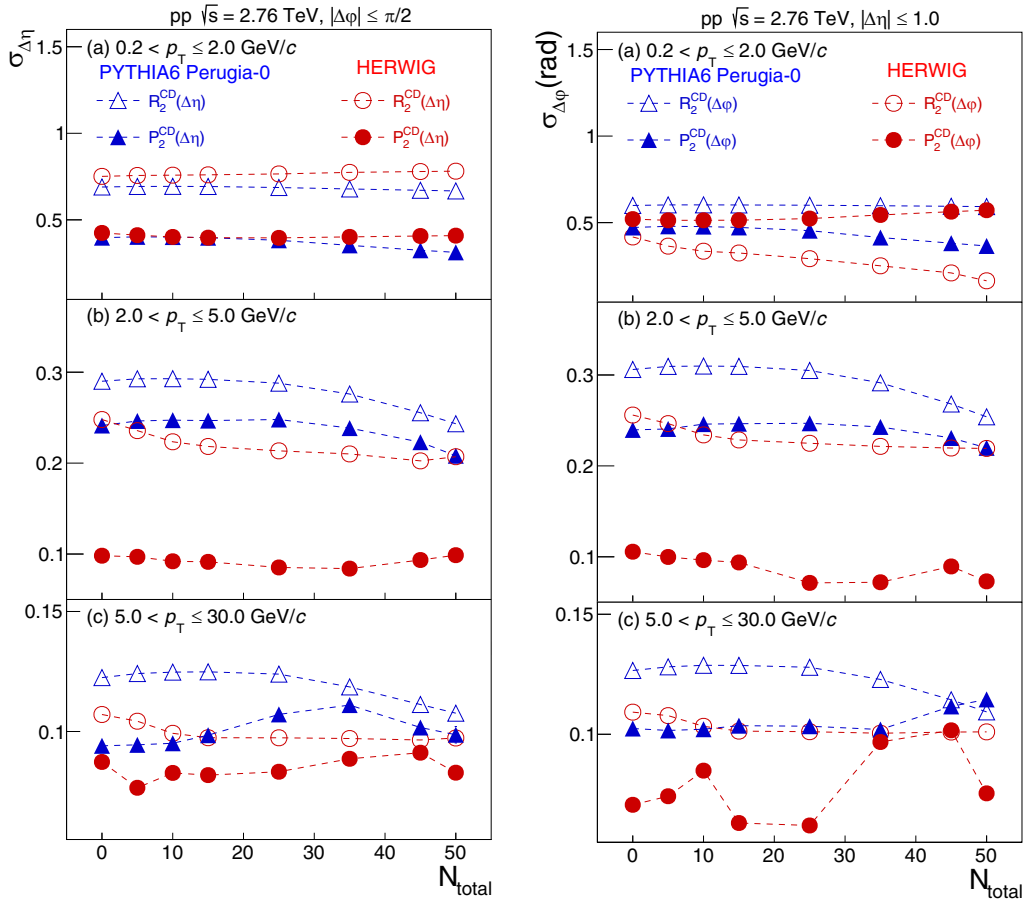

FIG. 15. Width of the near-side peak of CD correlation functions along $\Delta\eta$ (left panel), in the range $|\Delta\varphi| \leqslant \pi/2$, and along $\Delta\varphi$ (right panel), in the range $|\Delta\eta| \leqslant 1.0$. Dotted lines are drawn to guide the eye.

$\Delta\varphi \sim \pi$ in R_2 correlation functions but produces a very large amplitude away-side in P_2. One also finds that PYTHIA and HERWIG produce away-side ridges with different shapes and strengths as well as quantitatively different p_T dependence. Comparative measurements of the R_2 and P_2 correlators in different particle momentum ranges in pp collisions should thus provide additional insight and constraints on the hadronization mechanisms implemented in these models.

2. *Charge-dependent correlations*

We next shift our attention to the CD correlation functions presented in Figs. 7 and 9, and their projections in Figs. 10 and 11.

These were obtained by subtraction of the LS correlations from the US correlations according to Eq. (9). As such, they emphasize the role of charge conservation in particle production. Correlation functions R_2 (and similarly charge balance functions) indeed provide signatures of the charged particle pair production and transport in pp and A–A collisions. For instance, at momenta in excess of 2.0 GeV/c, as shown in Figs. 7(b) and 7(c), one observes the correlator R_2 features an isolated peak centered at $(\Delta\eta, \Delta\varphi) = (0, 0)$ resulting from the fact that correlated charged particle production occurs almost exclusively within the confines of a single jet.

The width of the peak decreases monotonically with increasing particle momentum owing to the Schwinger mechanism and angular ordering discussed in Sec. II. At lower momenta, however, correlated charged pair production may occur over a wider range of angles, even back-to-back, as illustrated by the very sharp and narrow away-side ridge predicted by HERWIG in the range $0.2 \leqslant p_T \leqslant 2.0$ GeV/c. The R_2^{CD} correlation functions obtained with PYTHIA (top panels) and HERWIG (bottom panels) for particles in the range $0.2 \leqslant p_T \leqslant 2.0$ GeV/c indeed feature a more complicated shape involving both a near-side peak and an away-side structure. In this case, one notes that PYTHIA and HERWIG produce very different predictions, owing most likely to their different implementation of the underlying event. Additionally note, as exemplified in Fig. 7, that the shape and strength of R_2^{CD} exhibit a strong dependence on the produced hadron multiplicity. Measurements of R_2^{CD} in pp collisions for various momentum and produced particle multiplicity ranges shall then provide very useful constraints in the tuning of these models.

The PYTHIA and HERWIG predictions for P_2^{CD} correlation functions, shown in Fig. 9, indicate this correlator is also of interest to probe the internal structure of jets and the charge production ordering. With PYTHIA, the near-side peak of the P_2^{CD} correlation functions is significantly narrower

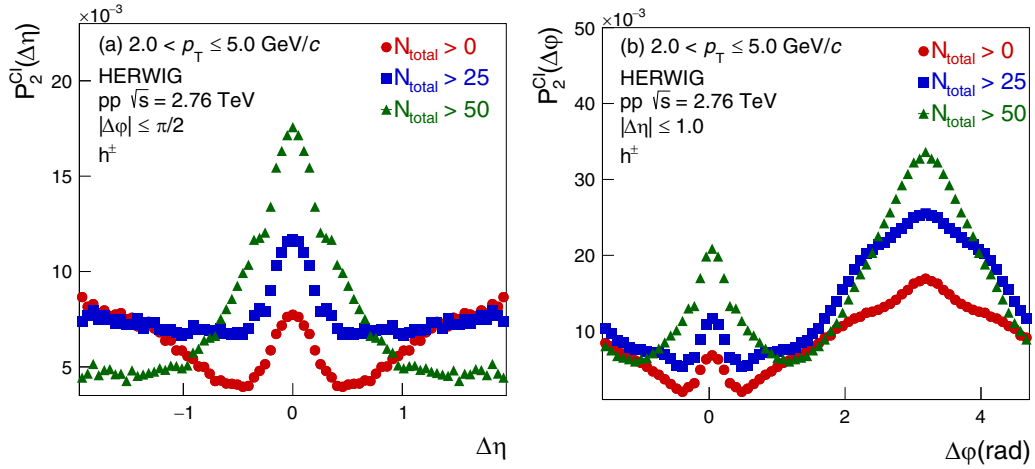

FIG. 16. Projections onto $\Delta\eta$ (left panel) and $\Delta\varphi$ (right panel) of the P_2^{CI} correlation functions calculated with HERWIG for $h^{\pm}$ in the p_T range 2.0–5.0 GeV/c in pp collisions at $\sqrt{s} = 2.76$ TeV for 3 different N_{total} cuts. The $\Delta\eta$ and $\Delta\varphi$ projections are calculated as averages of the two-dimensional correlations in the ranges $|\Delta\varphi| \leqslant \pi/2$ and $|\Delta\eta| \leqslant 1.0$, respectively.

than its R_2^{CD} counterpart in the lowest p_T range considered, but somewhat wider at higher p_T. By contrast, HERWIG's predictions of P_2^{CD} features a somewhat narrower near-side peak in all three momentum ranges. One also notes that the near-side predicted by PYTHIA and HERWIG have different shapes, widths, and a somewhat complicated dependence on the p_T of the particles. One finds additionally that the away-side of P_2^{CD} correlation functions feature a large amplitude for high-p_T particles. This is in stark contrast to the R_2^{CD} correlation functions that feature an almost flat away-side yield. Such a small away-side yield is expected in R_2^{CD} owing to the fact that particle production above $p_T \geqslant 2$ GeV/c is dominated by jet fragmentation. Given charge is conserved locally in the jet fragmentation process, one can expect, on general grounds, that charge correlations between jets, if any, are driven primarily by the charge of the parton that initiate the jets. Quark jets may be charge correlated but jets initiated by gluons should not be, at least to first order. Measurements of the P_2^{CD} away-side strength thus provide an additional tool to probe the nature of the jets measured in pp and A–A collisions. Indeed, back-to-back gluon jets should yield no contributions to the away-side of P_2^{CD} correlation functions but quark-quark jet pairs should have a finite CD correlation. The measured away-side yield of P_2^{CD} correlation functions may thus provide a new tool to determine the origin and nature of jets measured in elementary collisions.

We note that the R_2^{CD} correlator computed with HERWIG in the range $0.2 < p_T \leqslant 2.0$ GeV/c, shown in Fig. 7, features a narrow elongated structure at $\Delta\varphi = \pi$. This structure likely corresponds to underlying event particle pairs emitted back-to-back in the laboratory frame and are likely produced in excess given such a structure is not observed in data reported by the ALICE collaboration [28]. We find, however, that contributions of such pairs to the correlator are suppressed in HERWIG events featuring a total particle multiplicity $N_{total} > 50$ in the fiducial acceptance, as shown in Fig. 8. An experimental investigation of R_2^{CD} and P_2^{CD} correlation functions as a function of pp collision multiplicity is thus of obvious interest

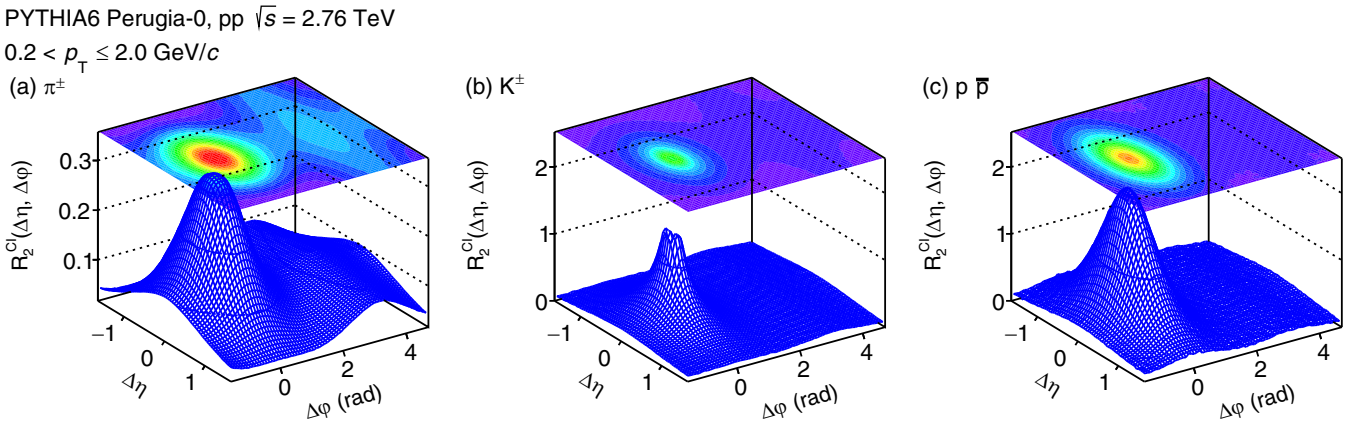

FIG. 17. Correlation functions R_2^{CI} of $\pi^{\pm}$, $K^{\pm}$ and $p\bar{p}$, within $|\eta| < 1.0$ and $0.2 < p_T \leqslant 2.0$ GeV/c, obtained with PYTHIA in pp collisions at $\sqrt{s} = 2.76$ TeV.

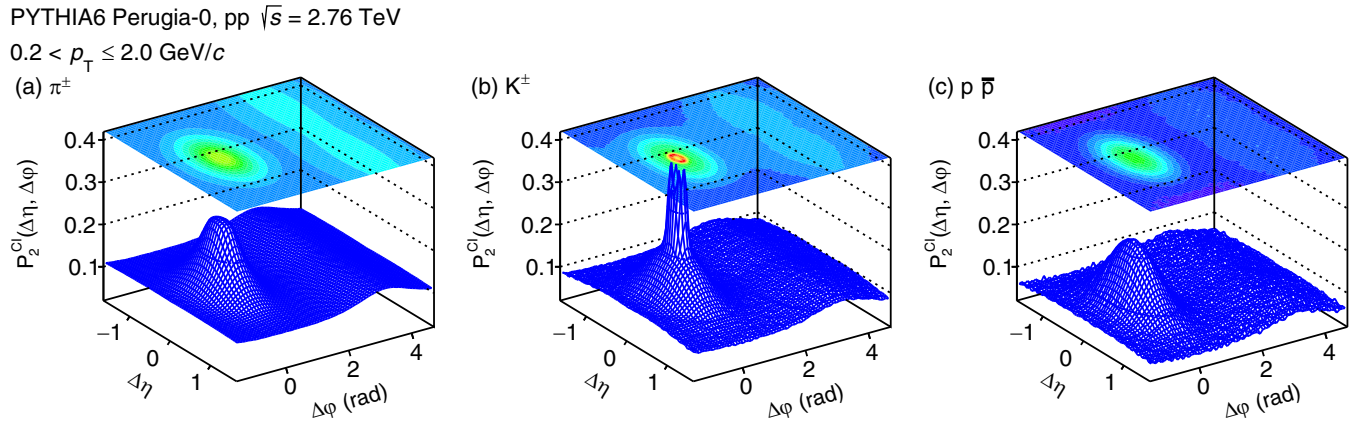

FIG. 18. Correlation functions P_2^{CI} of $\pi^{\pm}$, $K^{\pm}$ and $p\bar{p}$, within $|\eta| < 1.0$ and $0.2 < p_T \leqslant 2.0\,\mathrm{GeV}/c$, obtained with PYTHIA in pp collisions at $\sqrt{s} = 2.76\,\mathrm{TeV}$.

to elucidate the role and interplay of underlying events and multi-jet production in these collisions.

B. Transverse momentum dependence of the width of the CI and CD near-side peaks

We study the p_T evolution of the RMS widths of the near-side peaks of the R_2 and P_2 correlation functions obtained with PYTHIA and HERWIG. The $\Delta\eta$ and $\Delta\varphi$ RMS widths are calculated according to

$$\sigma_{\Delta\eta} = \left(\frac{\sum_{i,j}[O(\Delta\eta_i, \Delta\varphi_j) - O_{\mathrm{offset}}]\Delta\eta_i^2}{\sum_{i,j} O(\Delta\eta_i, \Delta\varphi_j)} \right)^{1/2}, \quad (11)$$

$$\sigma_{\Delta\varphi} = \left(\frac{\sum_{i,j}[O(\Delta\eta_i, \Delta\varphi_j) - O_{\mathrm{offset}}]\Delta\varphi_i^2}{\sum_{i,j} O(\Delta\eta_i, \Delta\varphi_j)} \right)^{1/2}, \quad (12)$$

where $O(\Delta\eta_i, \Delta\varphi_j)$ represent the strength of the correlation functions in bins $\Delta\eta_i$ and $\Delta\varphi_j$ and the sums on $\Delta\eta_i$ covers the $|\Delta\eta| \leqslant 1.0$ acceptance of the simulation, whereas the sums on $\Delta\varphi_i$ are limited to exclude the away-side ridge. Offsets are used to suppress negative correlation values and eliminate trivial width values determined by the breadth of the acceptance. They are obtained by taking the average of three bins at the edge of the acceptance, i.e., at $|\Delta\eta| = 2.0$ for $\Delta\eta$ projections, and at the minimum of the correlations, near $\Delta\varphi = -\pi/2$, for $\Delta\varphi$ projections. The three-bin average technique is also used for calculating offsets whenever undershoots are present in P_2 correlators.

Figures 12 and 13 present plots of the evolution of the $\Delta\eta$ and $\Delta\varphi$ widths of the near-side peak of CI and CD correlators as a function of p_T. Overall, one finds the widths decrease with rising p_T. However, widths obtained with PYTHIA exhibit a smooth and monotonic behavior with increasing particle p_T whereas widths obtained from HERWIG exhibit a more complicated p_T dependence. This study reveals an interesting case where the P_2 width is broader than that of R_2 in some p_T ranges, in stark contrast with the results reported in Ref. [28].

To further understand the structures observed in R_2 and P_2 correlation functions presented in Figs. 3–9, we study, in Figs. 14 and 15, the evolution of the near-side peak of the correlators as a function of the total particle multiplicity N_{total}. We find that the longitudinal and azimuthal widths, $\sigma_{\Delta\eta}$ and $\sigma_{\Delta\varphi}$, of the R_2^{CI}, R_2^{CD}, and P_2^{CD} correlators are slowly varying functions of N_{total}, with largest dependence observed for the

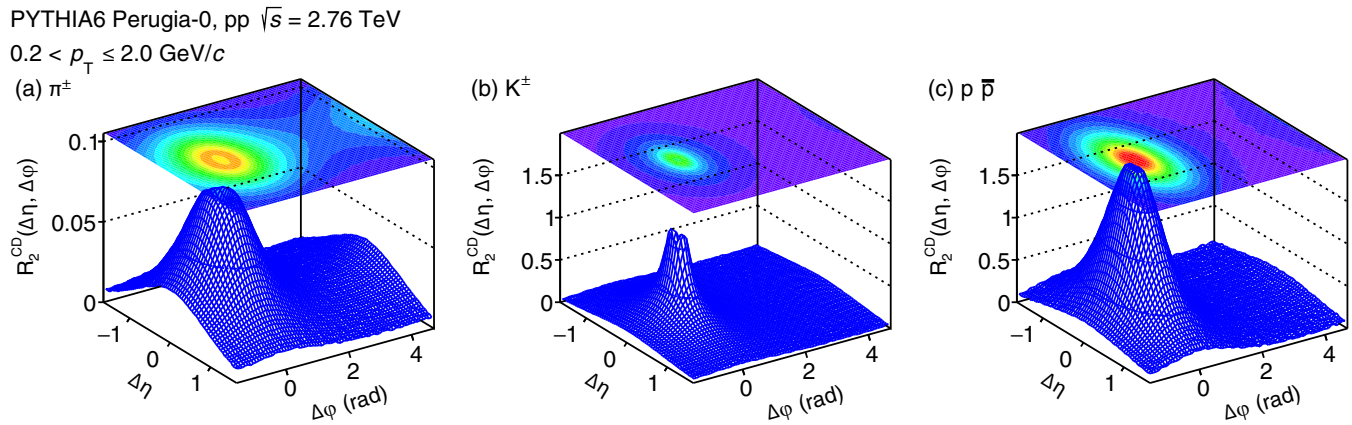

FIG. 19. Correlation functions R_2^{CD} of $\pi^{\pm}$, $K^{\pm}$ and $p\bar{p}$, within $|\eta| < 1.0$ and $0.2 < p_T \leqslant 2.0\,\mathrm{GeV}/c$, obtained with PYTHIA in pp collisions at $\sqrt{s} = 2.76\,\mathrm{TeV}$.

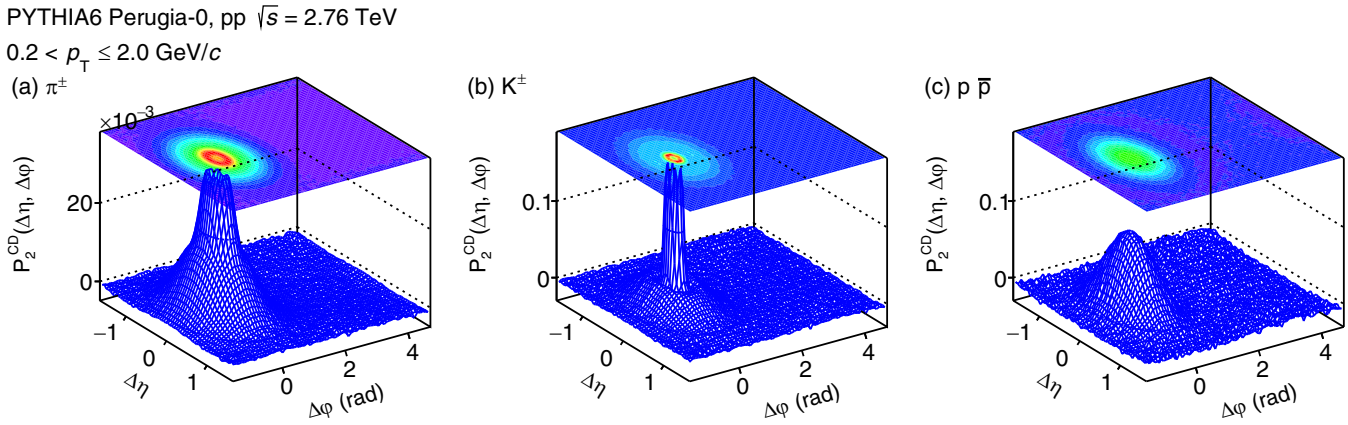

FIG. 20. Correlation functions P_2^{CD} of $\pi^{\pm}$, $K^{\pm}$ and $p\bar{p}$, within $|\eta| < 1.0$ and $0.2 < p_T \leqslant 2.0\,\mathrm{GeV}/c$, obtained with PYTHIA in pp collisions at $\sqrt{s} = 2.76\,\mathrm{TeV}$.

width $\sigma_{\Delta\varphi}$ predicted by HERWIG for particles in the range $0.2 < p_T \leqslant 2.0\ \mathrm{GeV}/c$. The widths of the P_2^{CI} correlator, on the other hand, exhibit a more complicated dependence on N_{total}. One observes, indeed, that the widths extracted both from PYTHIA and HERWIG exhibit a discontinuity near or above $N_{\mathrm{total}} = 30$, thereby signaling a drastic change in the shape of these correlation functions between low and high multiplicity events. The shape dependence on N_{total} is illustrated in Fig. 16. Events of low multiplicity feature P_2^{CI} correlator with a clear undershoot structure, yielding narrow widths in both the longitudinal and azimuthal directions. As argued above, the undershoot structure is associated with the production of pairs featuring $\Delta p_T \Delta p_T < 0$ but multiplicity fluctuations shift the correlator, globally, to positive values. The number of such pair combinations is manifestly reduced, however, for collisions with large N_{total}. These consequently do not feature an undershoot behavior and thus produce a broad near-side peak. This behavior likely stems from the fact that high-multiplicity events favor gluon jets. These are less collimated than quark jets and feature softer particles on average [52]. Evidently, such variations are not possible with the R_2^{CI} correlators. We thus conclude that the P_2^{CI} correlator

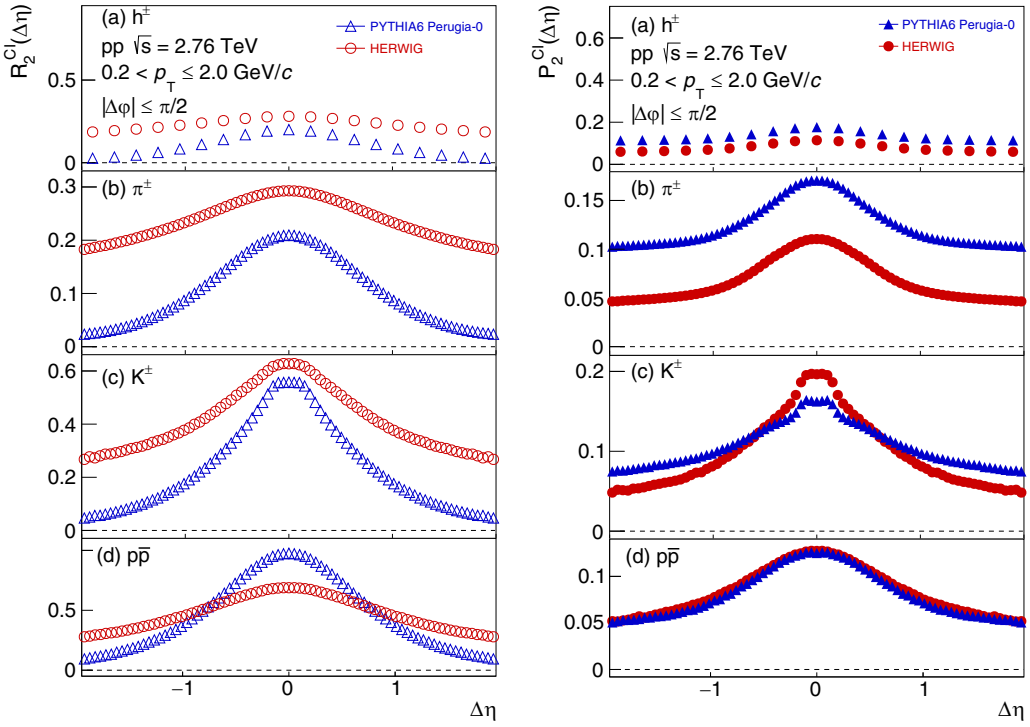

FIG. 21. Projections onto $\Delta\eta$ of R_2^{CI} (left column) and P_2^{CI} (right column) correlation functions of $h^{\pm}$, $\pi^{\pm}$, $K^{\pm}$ and $p\bar{p}$ calculated with PYTHIA (blue) and HERWIG (red) in pp collisions at $\sqrt{s} = 2.76\,\mathrm{TeV}$. The projections are calculated as averages of the two-dimensional correlations in the range $|\Delta\varphi| \leqslant \pi/2$.

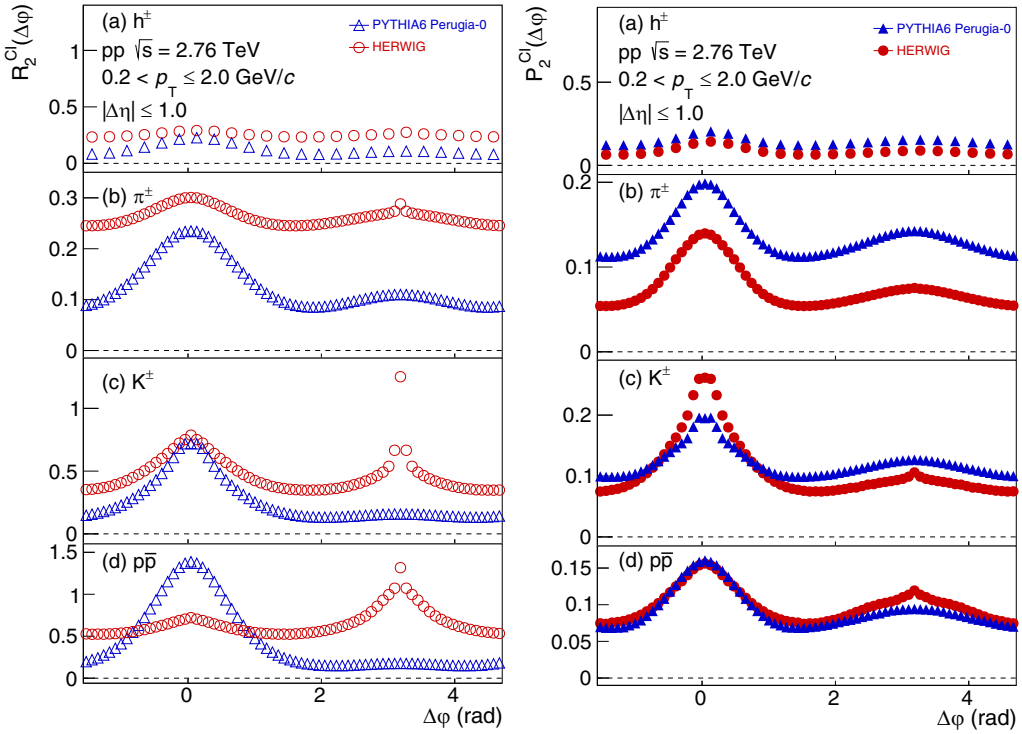

FIG. 22. Projections onto $\Delta\varphi$ of R_2^{CI} (left column) and P_2^{CI} (right column) correlation functions of $h^{\pm}$, $\pi^{\pm}$, $K^{\pm}$ and $p\bar{p}$ calculated with PYTHIA (blue) and HERWIG (red) in pp collisions at $\sqrt{s} = 2.76$ TeV.

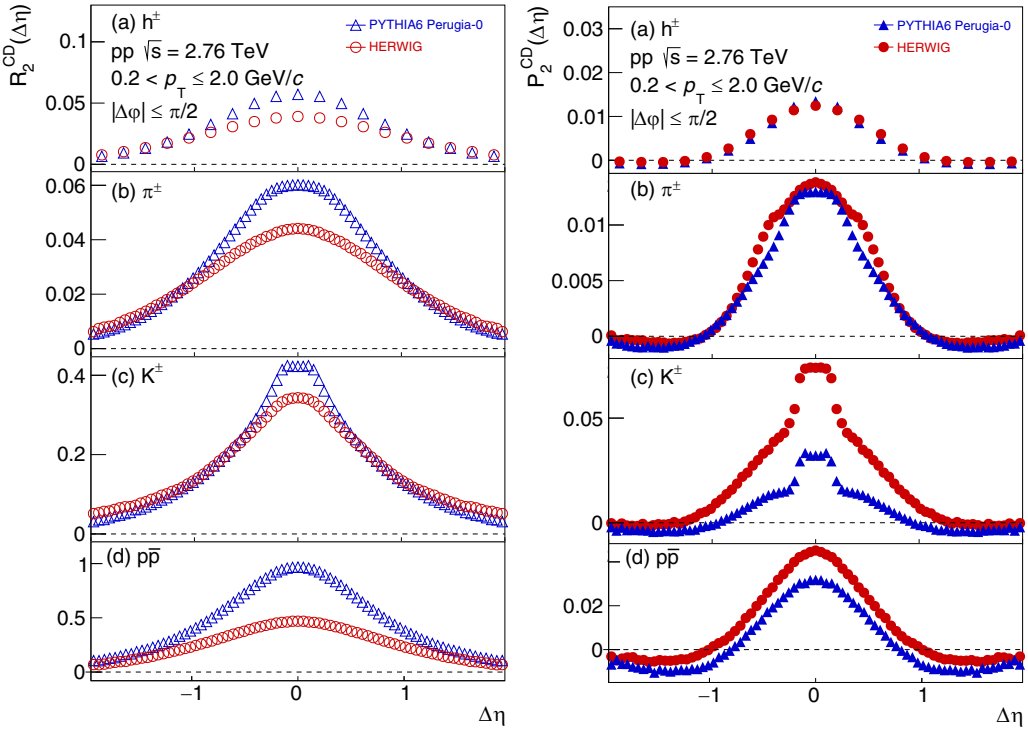

FIG. 23. Projections onto $\Delta\eta$ of R_2^{CD} (left column) and P_2^{CD} (right column) correlation functions of $h^{\pm}$, $\pi^{\pm}$, $K^{\pm}$ and $p\bar{p}$ calculated with PYTHIA (blue) and HERWIG (red) in pp collisions at $\sqrt{s} = 2.76$ TeV. The projections are calculated as averages of the two-dimensional correlations in the range $|\Delta\varphi| \leqslant \pi/2$.

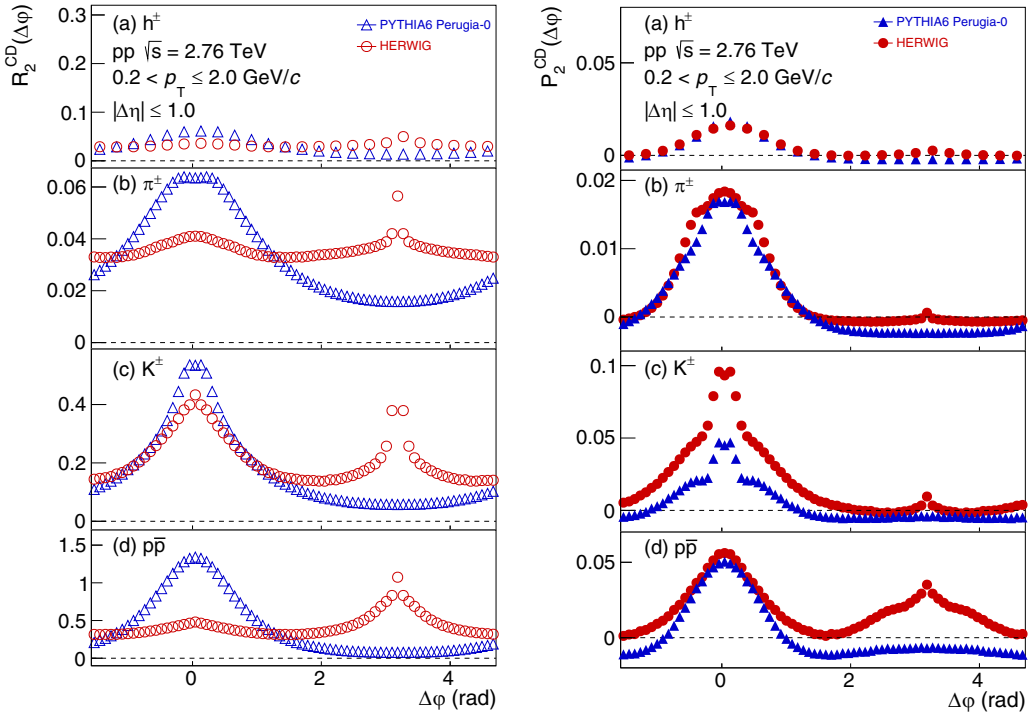

FIG. 24. Projections onto $\Delta\varphi$ of R_2^{CD} (left column) and P_2^{CD} (right column) correlation functions of $h^{\pm}$, $\pi^{\pm}$, $K^{\pm}$ and $p\bar{p}$ calculated with PYTHIA (blue) and HERWIG (red) in pp collisions at $\sqrt{s} = 2.76$ TeV.

constitutes a more discriminating probe of the correlation structure of jets and their underlying events than the R_2^{CI} correlator.

C. Identified charged hadron correlations

Experimental studies at the ISR, FNAL, and the LHC have shown that jet fragmentation functions of identified species vary appreciably between mesons and baryons as well as with their quark content ([53] and references therein). Unfortunately, measuring the fragmentation functions of identified hadron species within jets is a statistically onerous and difficult task, specially for high-z particles in high-energy jets. Measuring the strength and shape of R_2^{CI}, P_2^{CI}, R_2^{CD}, and P_2^{CD} correlation functions of identified high-p_T hadrons, however, may provide an invaluable proxy to such studies. We proceed to substantiate this hypothesis by studying the shape and strength of identified hadron correlation functions based on predictions by the PYTHIA and HERWIG models. Figures 17 and 18, respectively, display R_2^{CI} and P_2^{CI} correlation functions calculated with PYTHIA for $\pi^{\pm}$, $K^{\pm}$ and $p\bar{p}$, in the range $0.2 < p_T \leqslant 2.0$ GeV/c.

Again, in the case of identified particles, one observes that the width of the near-side peak of the P_2^{CI} correlator is significantly narrower than its R_2^{CI} counterpart. However, the shape and width of these two correlators do not exhibit a monotonic dependence on the mass of the particles. For kaons, in particular, both R_2^{CI} and P_2^{CI} feature a near-side peak that might be perhaps best described by a superposition of a wide and a narrow Gaussian peak, which arises, in part, from a strong admixture of ϕ-meson decays. A similar situation arises for R_2^{CD} and P_2^{CD} shown in Figs. 19 and 20, respectively. One finds, for all three particle species, that the near-side peak of the P_2^{CD} correlators are markedly narrower than their R_2^{CD} counterparts. One also observes that the kaon near-side peaks are much narrower than those of pions and protons. It is also worth noticing that the pion R_2^{CD} correlator shows a rather large away-side amplitude (relative to its near-side peak amplitude) while kaons and protons feature much smaller relative away-side amplitudes for this correlator. By contrast, all three species have a flat and nearly vanishing away-side amplitude in P_2^{CD} within PYTHIA simulations (Fig. 20) for particles within $0.2 < p_T \leqslant 2.0$ GeV/c. Qualitatively similar conclusions are obtained from calculations of the R_2 and P_2 correlators with HERWIG in this momentum range (2D plots not shown). Indeed, projections of the R_2 and P_2 correlation functions obtained with PYTHIA and HERWIG, shown in Figs. 21–24, illustrate that while the predictions of the two models are qualitatively similar, they differ quantitatively for the three particle species considered. It is very difficult to study this in other p_T regions for RMS width calculation because of large oscillating behavior in P_2^{CD} $p\bar{p}$ in the p_T range 2.0–5.0 GeV/c. An actual measurement of such correlation functions (possible at the LHC with the ALICE detector) shall thus provide significant constraints to tune these models and achieve a better understanding of particle production processes in elementary particle collisions.

V. SUMMARY

We presented a study of charge-independent and charge-dependent two-particle differential- number correlation

functions R_2 and transverse momentum correlation functions P_2 in pp collisions at $\sqrt{s} = 2.76$ TeV with the PYTHIA and HERWIG Monte Carlo models. Calculations were presented for unidentified hadrons as well as for $\pi^{\pm}$, $K^{\pm}$ and $p\bar{p}$ individual species in selected ranges of transverse momentum. PYTHIA and HERWIG both qualitatively reproduce the near-side peak and away-side ridge correlation features reported by experiments. At low p_T, both models produce narrower near-side peaks in P_2 correlations than in R_2 as reported by the ALICE collaboration in p–Pb and Pb–Pb collisions [28]. This suggests that the narrower shape of the P_2 near-side peak is largely determined by the p_T dependent angular ordering of hadrons produced in jets, as discussed in Sec. II. We have provided detailed calculations of the longitudinal and azimuthal widths of the near-side peak as a reference to prospective experimental studies of these correlation functions. Both PYTHIA and HERWIG predict widths that decrease with increasing p_T. Widths extracted for P_2 correlators are typically significantly narrower than those of the R_2 counterparts. We also showed that the models predict non-trivial dependence on the mass of identified particles arising in part from resonance decays.

We additionally find that the models produce large amplitude ridge structures at $\Delta\varphi = \pi$ in P_2 correlation functions while yielding relatively modest ridges in R_2. The amplitude of the ridge structure in P_2^{CI} is found to increase with the particle p_T range considered reaching rather large amplitude for particles in the $5.0 < p_T \leqslant 30.0\,\text{GeV}/c$ range. An away-side ridge is also observed in P_2^{CD} correlation functions. The magnitude of this ridge shall depend on jet-to-jet charge correlations. Measurements of P_2^{CD} correlation functions of high-p_T particles in pp collisions might then be sensitive to the charge of the partons initiating the observed jets. Elucidation of this conjecture, however, requires further studies, with both PYTHIA and HERWIG, of the correlation functions obtained when jet production is restricted to gluon-gluon or quark-quark processes.

ACKNOWLEDGMENTS

The authors thank Drs. Joern Putschke and Sidharth Prasad for fruitful discussions and their invaluable review of the manuscript. This work was supported in part by the United States Department of Energy, Office of Nuclear Physics (DOE NP), United States of America, under Grant No. DE-FG02-92ER40713, and the Department of Science and Technology (DST), Government of India as well as the University Grants Commission (UGC), Government of India.

[1] J. Adams *et al.* (STAR Collaboration), Nucl. Phys. A **757**, 102 (2005).
[2] K. Adcox *et al.* (PHENIX Collaboration), Nucl. Phys. A **757**, 184 (2005).
[3] K. Aamodt *et al.* (ALICE Collaboration), Phys. Rev. Lett. **105**, 252302 (2010).
[4] K. Aamodt *et al.* (ALICE Collaboration), Phys. Lett. B **708**, 249 (2012).
[5] S. Chatrchyan *et al.* (CMS Collaboration), J. High Energy Phys. 02 (2014) 088.
[6] J. Adam *et al.* (ALICE Collaboration), Phys. Lett. B **762**, 376 (2016).
[7] S. Mohapatra, Measurement of the azimuthal anisotropy for charged particle production in Pb–Pb collisions at $\sqrt{s_{NN}} =$ 2.76 TeV and in p–Pb collisions at $\sqrt{s_{NN}} = 5.02$ TeV with the ATLAS detector at the LHC, Ph.D. thesis, SUNY, Stony Brook, 2013.
[8] A. Adare *et al.* (PHENIX Collaboration), Phys. Rev. Lett. **98**, 162301 (2007).
[9] B. B. Abelev *et al.* (ALICE Collaboration), J. High Energy Phys. 06 (2015) 190.
[10] J. Adam *et al.* (ALICE Collaboration), J. High Energy Phys. 09 (2016) 164.
[11] G. Aad *et al.* (ATLAS Collaboration), Phys. Rev. C **86**, 014907 (2012).
[12] S. Esumi (PHENIX Collaboration), PoS (CPOD2017) 018 (2018).
[13] S. Acharya *et al.* (ALICE Collaboration), Eur. Phys. J. C **77**, 569 (2017).
[14] X. Zhu (ALICE Collaboration), in *Proceedings of the Workshop on Hadron Nuclear Physics (HNP'13): Zhangjiajie, China, July 18–22, 2013* (2013); arXiv:1311.2394 [hep-ex].
[15] B. B. Abelev *et al.* (ALICE Collaboration), Phys. Rev. C **90**, 054901 (2014).
[16] C. Bernardes (CMS Collaboration), PoS (EPS-HEP2017) 155 (2017).
[17] A. M. Sirunyan *et al.* (CMS Collaboration), Phys. Rev. Lett. **121**, 082301 (2018).
[18] C. Adler *et al.* (STAR Collaboration), Phys. Rev. Lett. **90**, 082302 (2003).
[19] A. Adare *et al.* (PHENIX Collaboration), Phys. Rev. C **77**, 011901 (2008).
[20] S. Chatrchyan *et al.* (CMS Collaboration), Phys. Rev. C **84**, 024906 (2011).
[21] J. Adams *et al.* (STAR Collaboration), Phys. Rev. C **72**, 044902 (2005).
[22] H. Agakishiev *et al.* (STAR Collaboration), Phys. Lett. B **704**, 467 (2011).
[23] S. A. Bass, P. Danielewicz, and S. Pratt, Phys. Rev. Lett. **85**, 2689 (2000).
[24] S. Pratt, W. P. McCormack, and C. Ratti, Phys. Rev. C **92**, 064905 (2015).
[25] M. M. Aggarwal *et al.* (STAR Collaboration), Phys. Rev. C **82**, 024905 (2010).
[26] J. Adams *et al.* (STAR Collaboration), Phys. Rev. Lett. **90**, 172301 (2003).
[27] B. Abelev *et al.* (ALICE Collaboration), Phys. Lett. B **723**, 267 (2013).
[28] S. Acharya *et al.* (ALICE Collaboration), arXiv:1805.04422.
[29] J. Adam *et al.* (ALICE Collaboration), Phys. Rev. Lett. **118**, 162302 (2017).
[30] M. Sharma and C. A. Pruneau, Phys. Rev. C **79**, 024905 (2009).
[31] T. Sjostrand, S. Mrenna, and P. Skands, J. High Energy Phys. 05 (2006) 026.

[32] G. Corcella, I. Knowles, G. Marchesini, S. Moretti, K. Odagiri, P. Richardson, M. Seymour, and B. Webber, J. high Energy Phys. 01 (2001) 010.
[33] M. H. Seymour, AIP Conf. Proc. **357**, 568 (1996).
[34] M. Estienne, Phys. Atom. Nucl. **71**, 1535 (2008).
[35] B. Abelev *et al.* (ALICE Collaboration), Phys. Rev. D **91**, 112012 (2015).
[36] C. Pruneau, S. Gavin, and S. Voloshin, Phys. Rev. C **66**, 044904 (2002).
[37] P. Z. Skands, Phys. Rev. D **82**, 074018 (2010).
[38] T. Sjöstrand and P. Skands, Eur. Phys. J. C **39**, 129 (2005).
[39] M. Sandhoff and P. Skands, in *Proceedings of the Workshop on Physics at TeV Colliders, Les Houches, France, May 2–20, 2005* (2006); arXiv:hep-ph/0604120.
[40] A. Buckley, H. Hoeth, H. Lacker, H. Schulz, and J. E. V. Seggern, Eur. Phys. J. C **65**, 331 (2010).
[41] B. Andersson, G. Gustafson, G. Ingelman, and T. Sjostrand, Phys. Rept. **97**, 31 (1983).
[42] J. Pumplin, D. Stump, J. Huston, H. Lai, P. Nadolsky, and W. Tung, J. High Energy Phys. 07 (2002) 012.
[43] H. L. Lai, J. Huston, S. Kuhlmann, J. Morfin, F. Olness, J. F. Owens, J. Pumplin, and W. K. Tung, Eur. Phys. J. C **12**, 375 (2000).
[44] A. Mueller and W.-K. Tang, Phys. Lett. B **284**, 123 (1992).
[45] G. P. Salam, Acta Phys. Polon. B **30**, 3679 (1999).
[46] A. C. Diaz, G. C. Balbastre, and C. G. Trápaga, http://scielo.sld.cu/pdf/nuc/n50/nuc035011.pdf (2011).
[47] P. Csizmadia, P. Lévai, S. E. Vance, T. S. Biró, M. Gyulassy, and J. Zimányi, J. Phys. G: Nucl. Part. Phys. **25**, 321 (1999).
[48] D. Molnar and S. A. Voloshin, Phys. Rev. Lett. **91**, 092301 (2003).
[49] J. Adams *et al.* (STAR Collaboration), Phys. Rev. C **75**, 034901 (2007).
[50] B. I. Abelev *et al.* (STAR Collaboration), Phys. Rev. C **80**, 064912 (2009).
[51] A. Adare *et al.* (PHENIX Collaboration), Phys. Rev. C **78**, 014901 (2008).
[52] Y. K. Kim *et al.*, Phys. Rev. Lett. **63**, 1772 (1989).
[53] M. Tanabashi *et al.* (Particle Data Group), Phys. Rev. D **98**, 030001 (2018).